4. Results and Discussion

This chapter provides a detailed discussion on the observations and results obtained from the experiments described in Chapter 3 of the thesis. It is divided into four sections, corresponding to the four objectives of the study, presented in sequence from Sections 4.1 to 4.4.

Section 4.1 addresses the first objective, which involves examining the development and performance of the solar air heating system and the integrated solar greenhouse drying system under various climatic conditions. Section 4.2 presents findings related to the second objective, which focuses on the drying characteristics and quality evaluation of ginger using the developed dryer and drying modelling. Section 4.3 covers the third objective, providing insights into the thermal performance of the solar air heating system and the developed dryer, including CFD simulation and modelling. Finally, Section 4.4 discusses the fourth objective, which entails an environmental and economic analysis of the developed dryer.

4.1 Performance of solar air heating (SAH) and integrated solar greenhouse drying (ISGHD) system

The methodology chapter outlines the systematic approach employed in the development and evaluation of the corrugated type of solar air heating (SAH with PCM) and integrated solar greenhouse drying (ISGHD) system. This involved rigorous selection criteria based on performance metrics tailored to the specific objectives of the study. The experiment focused on determining the dryer's efficiency and the performance of the corrugated type of solar air heating (SAH with PCM) system. The experiment was conducted within the context of an integrated solar greenhouse drying system, wherein the SAH system, enhanced with phase change material (PCM) and photovoltaic (PV) modules to power essential components like blowers and exhausts, played a pivotal role in optimizing the ginger drying process. By meticulously designing the experiment to incorporate these elements, the aim was to achieve superior drying outcomes while leveraging sustainable and renewable energy sources. Through systematic experimentation and analysis, the methodology sought to elucidate the synergistic effects of integrating solar technologies with

traditional drying processes, ultimately contributing to the advancement of economic and eco-friendly agricultural drying practices.

4.1.1 Ambient parameters

Environmental variables are key in understanding how crops and food materials dry.

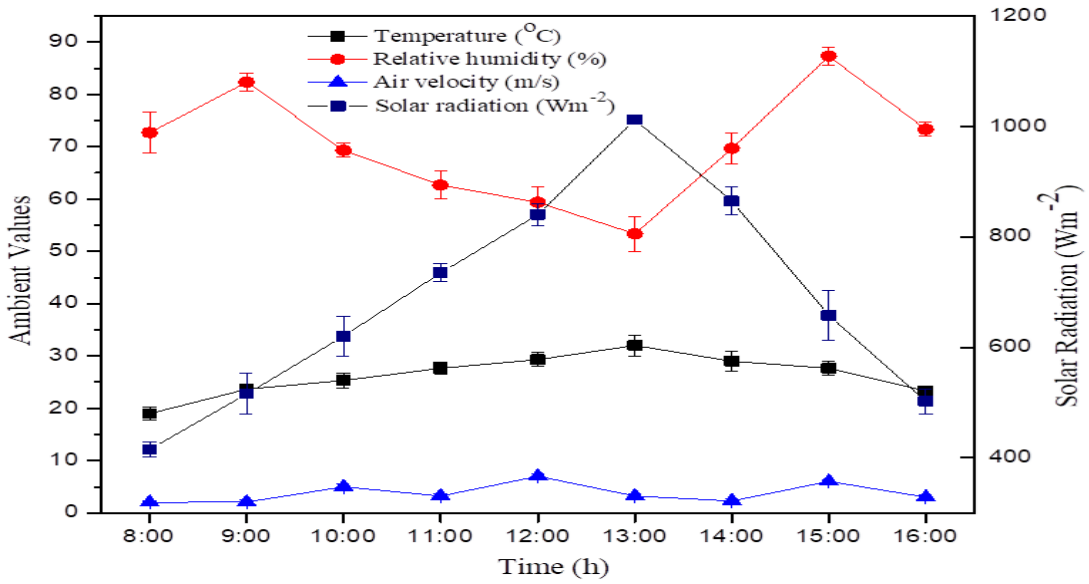

(a)

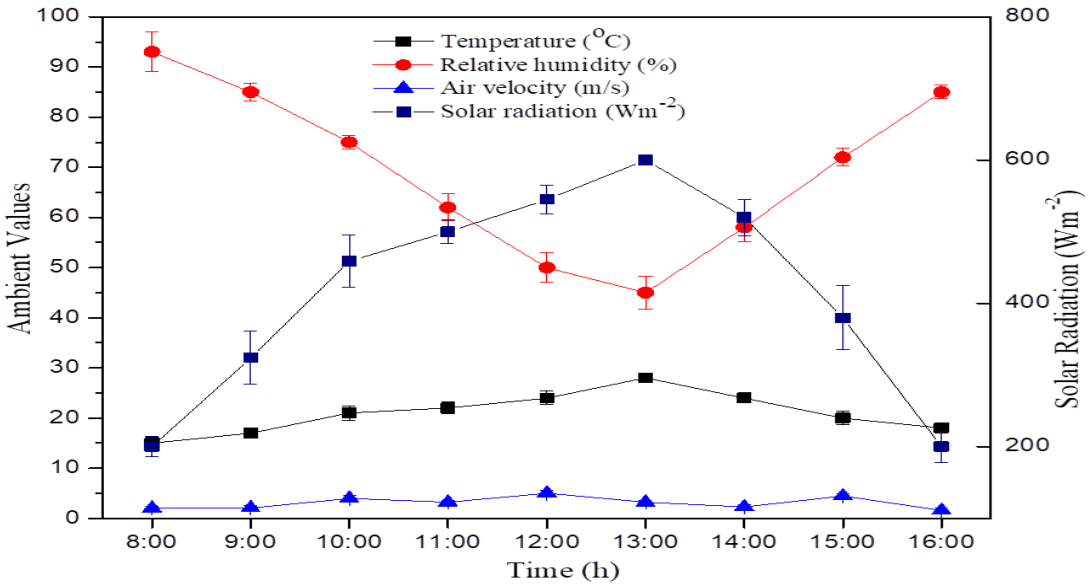

(b)

Fig. 4.1.1 Average of 20 days readings of ambient parameter during (a) Summer and (b) Winter seasons in the northeastern region

During summer (March 2021 to June 2021), strong solar radiation, ranging between 410 and 1020 Wm^{-2}, provides ample energy for efficient drying, while in winter (October 2021 to February 2021), it fluctuates between 200 and 590 Wm^{-2}.

Solar radiation intensity increases in the morning until noon then decreases until nightfall. Solar radiation fluctuated significantly each day during the drying period. The temperature of ambient air is crucial for drying. During summer, temperatures range from 19 °C to 33 °C, while in winter, they range from 15 °C to 27 °C. Relative humidity ranges from 55 to 92% in summer and 38 to 72% in winter. The lowest RH occurred between 12:00 and 1:00 p.m. due to the peak solar radiation increasing the temperature. Wind speed plays a role, too, with summer velocities ranging from 2.0 to 8.0 m/s and winter velocities from 1.0 to 5.0 m/s. Understanding these factors is essential for optimizing drying processes and preserving food effectively under different environmental conditions. Fig. 4.1.1 represents the ambient parameter during the summer and winter seasons in the northeastern region.

4.1.2 Even and span type solar greenhouse dryer structure

The parabolic SGHD structure has a higher average temperature than the even span SGHD, with a maximum solar radiation range of 200-420 Wm^{-2}, while the even span type ranges from 200-380 Wm^{-2}, observed between 12:00 to 1:00 p.m., as shown in Fig. 4.1.2.

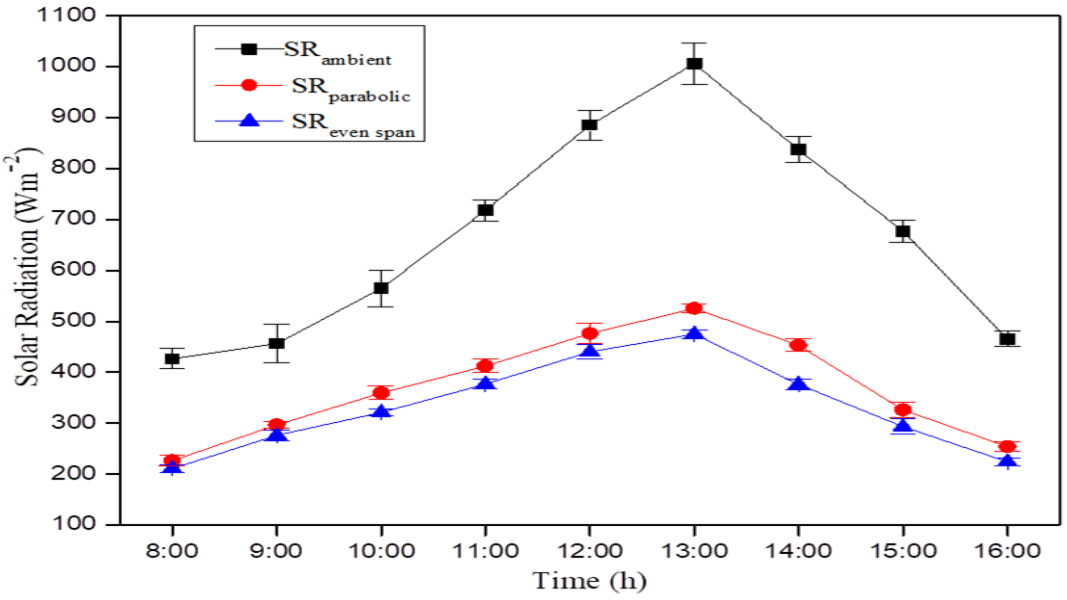

Fig. 4.1.2 Solar radiation variation in parabolic and even span solar greenhouse dryers

The choice of structure is pivotal in developing an efficient integrated solar greenhouse dryer, and the advantages conferred by the higher average temperature of the parabolic SGHD are notable. The parabolic design greatly enhances the dryer's thermal performance.

4.1.3 Efficiency of solar air heating (SAH) system

The corrugated type of solar air heater (SAH with PCM) demonstrates a superior highest output temperature of 73 °C, outperforming the flat type solar air heater (SAH), which reaches 58 °C, particularly at 12:00 to 1:00 p.m., as shown in Fig. 4.1.3. This temperature disparity can be attributed to the unique design of corrugations in the SAH, which induces turbulence in the airflow. This turbulence results in enhanced mixing and improved heat transfer efficiency. The corrugated structure promotes a more effective exchange of heat, allowing the SAH to achieve higher temperatures compared to its flat counterpart. The observed temperature difference underscores the importance of design considerations, emphasizing how the incorporation of corrugations positively influences the thermal performance and overall efficiency of SAH. In corrugated-type solar air heaters (SAH), the inclusion of phase change material (PCM) enhances efficiency by prolonging drying periods even after sunlight hours. This innovative feature ensures a consistent temperature rise and reduction in relative humidity during nighttime.

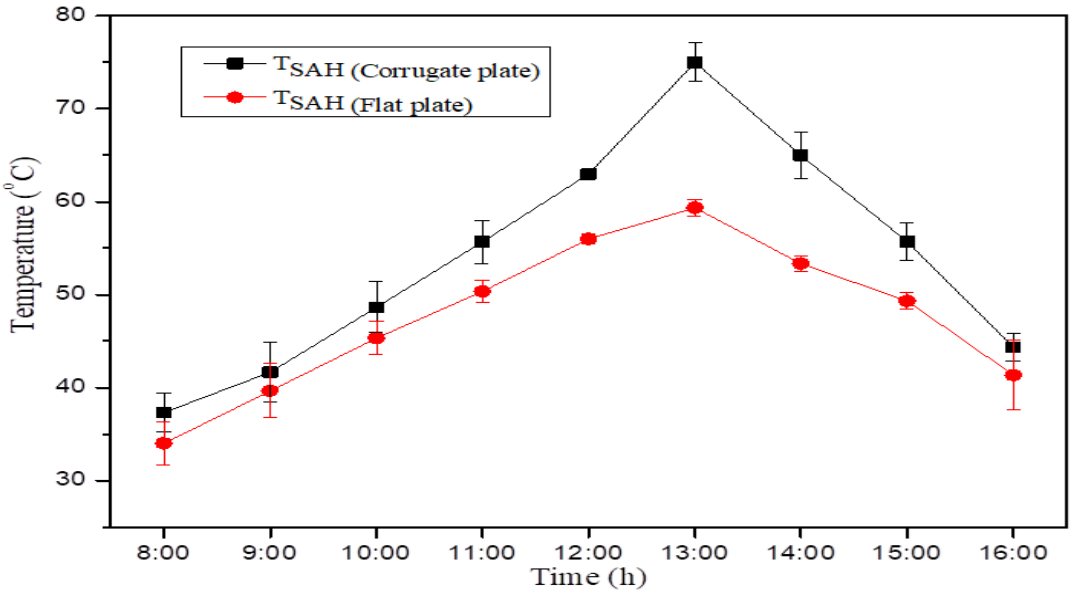

Fig. 4.1.3 Variation of outlet temperature on corrugate and flat type solar air heater

4.1.4 Efficiency of integrated solar greenhouse drying (ISGHD) system

During experiments, the corrugated solar air heating system exhibited outlet temperatures ranging from 35 to 75 °C, correlating with higher solar intensity and low air velocity between 12:00 to 1:00 p.m. Concurrently, the drying chamber temperature varied from 31 to 57 °C, aligning with fluctuations in solar radiation intensity. Notably, peak temperatures occurred during the period of maximum solar radiation intensity, as depicted in Fig. 4.1.4, illustrating the temperature variations in both the corrugated SAH and developed ISGHD system.

In this research, temperature and relative humidity were measured across various drying modes for ginger, including open sun drying (OSD), solar greenhouse drying (SGHD) in passive mode, and an integrated solar greenhouse drying system (ISGHD) in active mode featuring assisted corrugated solar air heating (SAH with PCM) and PV module assistance. (Fig. 4.1.5) illustrates the temperature variations in OSD (Natural convection), SGHD (Passive Mode), and ISGHD (Active Mode). Throughout the experiment, temperatures ranged from 19 to 33 °C in OSD, 21 to 39 °C in SGHD, and notably, 30 to 62 °C in ISGHD, observed between 8:00 a.m. to 4:00 p.m., peaking at 12:00 to 1:00 p.m. The ISGHD system achieved maximum temperatures conducive to efficient drying, significantly reducing drying time compared to other methods, thus demonstrating enhanced effectiveness and efficiency.

Relative humidity is a crucial parameter in drying processes, significantly influencing their efficiency and effectiveness. In a recent experiment comparing three drying methods, open Sun drying (OSD), solar greenhouse dryer (SGHD), and integrated solar greenhouse dryer (ISGHD), relative humidity varied within specific ranges. Throughout the experiment, relative humidity ranged from 56% to 93% during OSD, 42% to 78% during SGHD, and 18% to 68% during ISGHD. These variations were observed between 8:00 a.m. and 4:00 p.m., with the lowest relative humidity occurring typically between 12:00 and 1:00 p.m. Interestingly, the results highlighted that the lowest relative humidity levels contributed to better drying performance and increased efficiency across all drying methods. This finding underscores the importance of controlling relative humidity levels to optimize drying processes and enhance overall performance. (Fig. 4.1.6) represents the variation of relative humidity in OSD, SGHD and ISGHD drying methods.

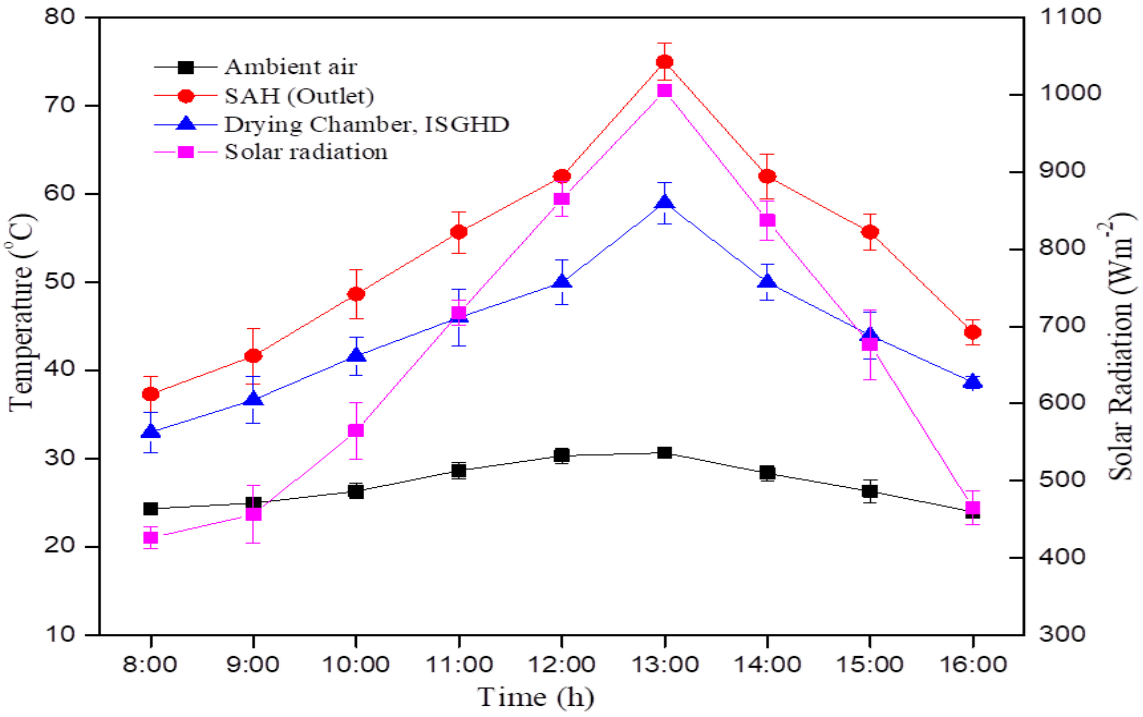

Fig. 4.1.4 Variation of temperature in corrugated type (SAH with PCM) and ISGHD with respect to solar radiation

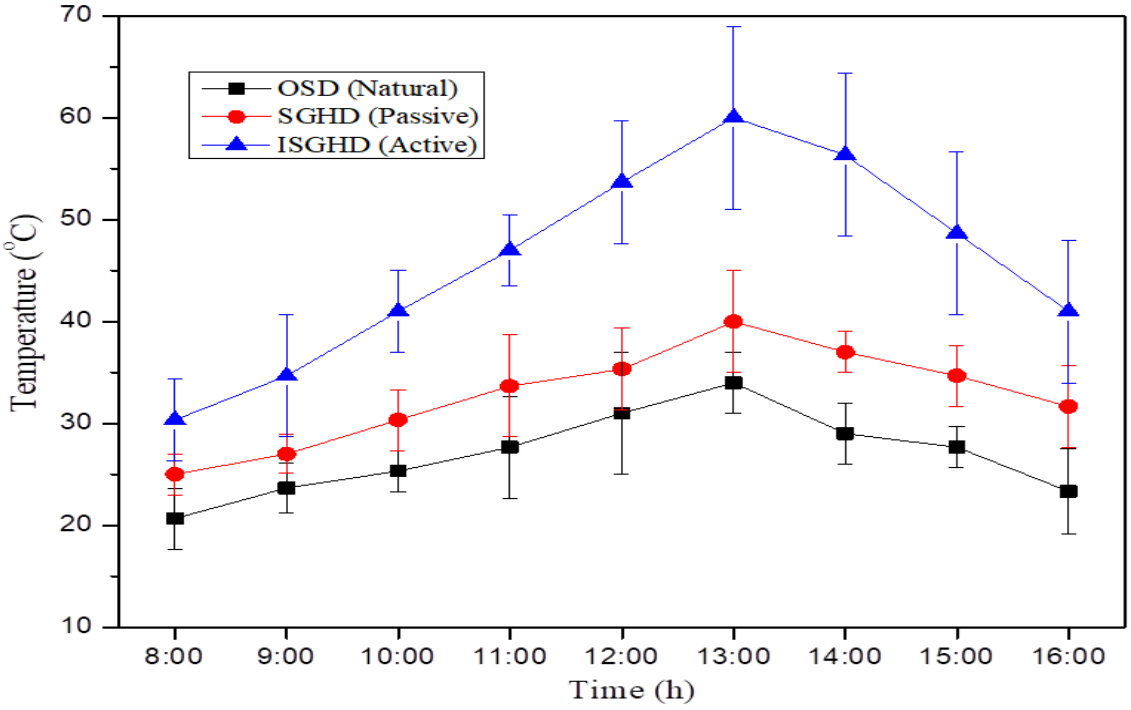

Fig. 4.1.5 Variation of temperature in OSD (Natural convection), SGHD (Passive Mode) and ISGHD (Active Mode) drying method

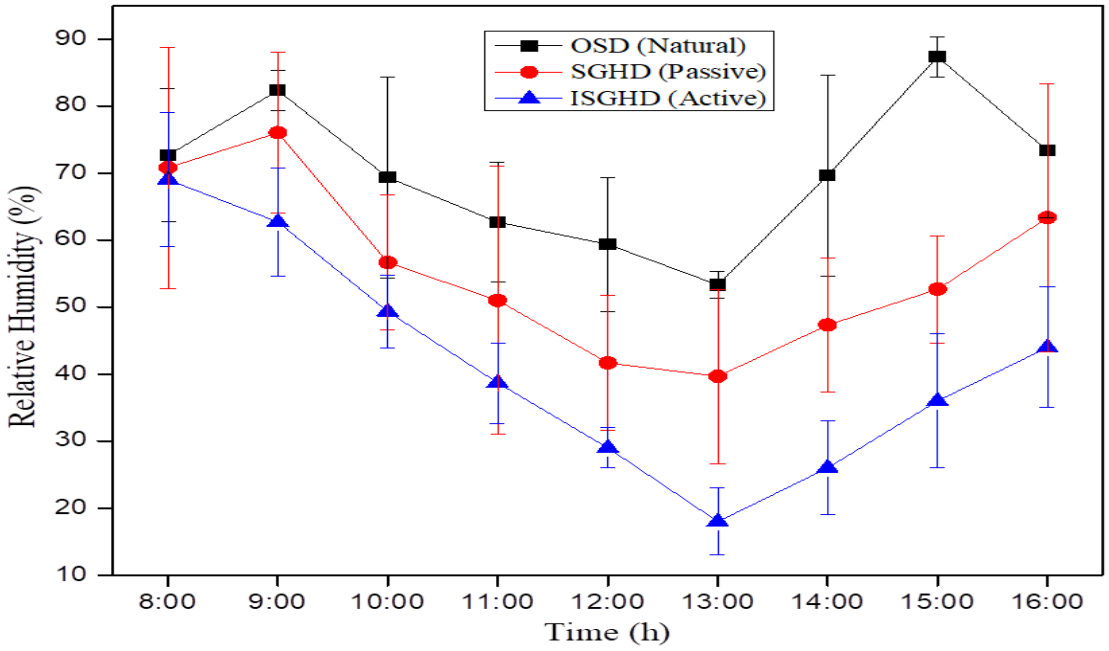

Fig. 4.1.6 Variation of relative humidity in OSD, SGHD and ISGHD drying method

4.1.5 Thermal energy storage (TES)

4.1.5.1 Sensible heat storage (SHS) system

The integrated solar greenhouse dryer achieves a temperature varies from 26 to 54 °C without a sensible heat storage (SHS) system. Introducing an SHS system increases the temperature ranged from 27 to 58 °C, improving the drying chamber's internal temperature by 2-3 °C, as shown in Fig. 4.1.7.

4.1.5.2 Latent heat storage (LHS) system

The performance of integrated solar greenhouse drying (ISGHD) system with and without phase change material (PCM) integration was evaluated based on temperature and relative humidity measurements during charging and discharging periods. In the case of ISGHD without PCM, the temperature ranged from 28 to 52 °C during charging and 22 to 25 °C during discharging. On the other hand, the ISGHD with PCM exhibited higher temperatures, ranging from 31 to 56 °C during charging and 25 to 29 °C during discharging. The introduction of PCM effectively increased drying duration by 3-4 hours when sunlight was not available, showcasing its role in extending the operational window of solar drying systems as shown in Fig. 4.1.8.

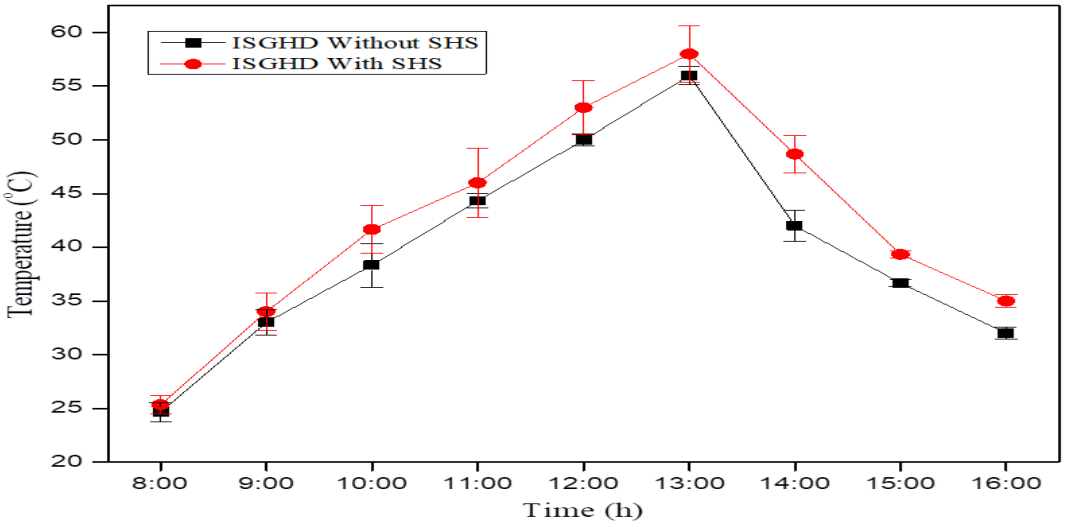

Fig. 4.1.7 Variation of temperature under ISGHD with and without sensible heat storage (SHS)

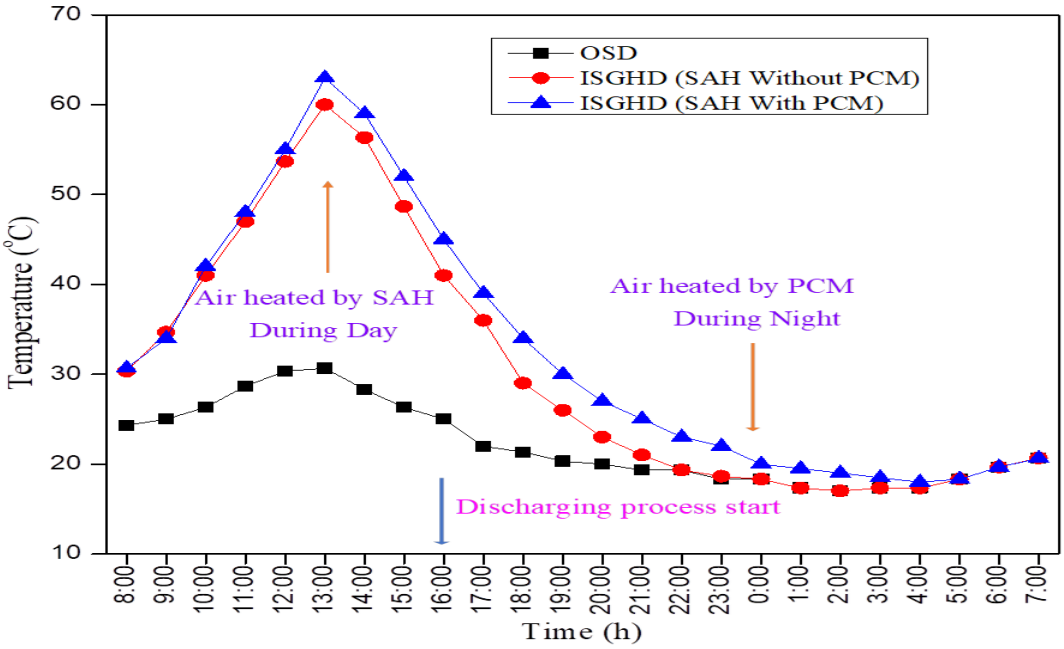

Fig. 4.1.8 Variation of temperature under OSD and inside drying chamber, ISGHD at SAH with and without PCM

Furthermore, the ISGHD without PCM experienced relative humidity levels between 17 to 70% during charging and 30 to 92% during discharging, as shown in Fig. 4.1.9. In contrast, the ISGHD with (SAH with PCM) showed slightly lower relative humidity levels, ranging from 14 to 70% during charging and 28 to 81% during discharging. This indicates that PCM integration contributes

to maintaining favourable humidity conditions for the drying process. Overall, the PCM-assisted solar air heating system not only enhances temperature control but also significantly extends the drying duration, making it a promising technology for increasing the efficiency of solar drying systems, particularly in situations where sunlight is intermittent or not available for extended periods.

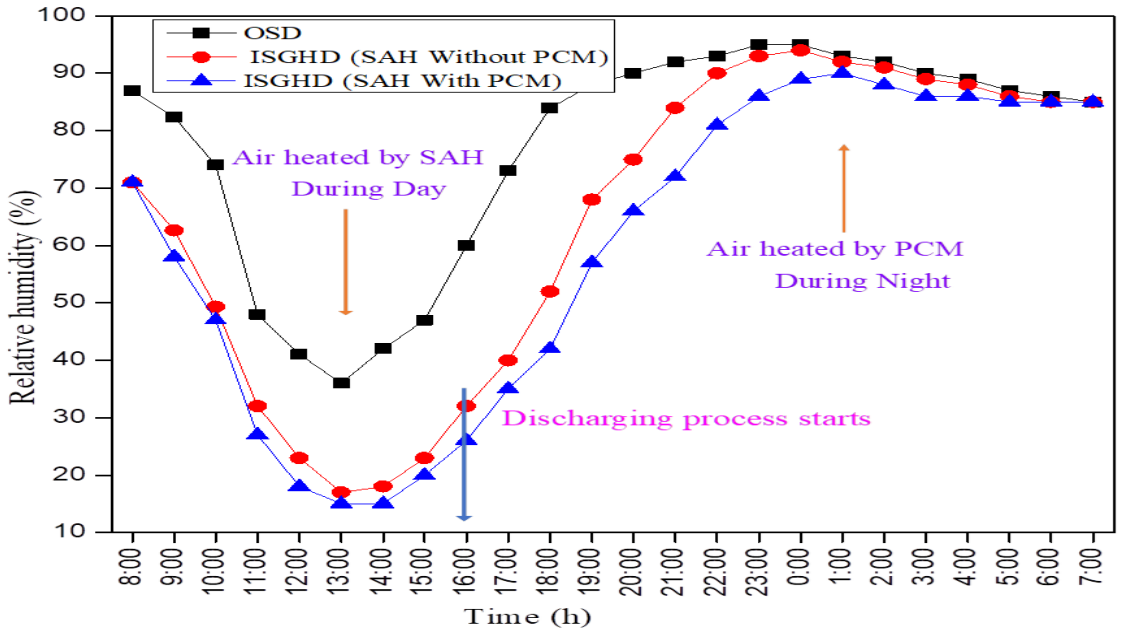

Fig. 4.1.9 Variation of relative humidity under OSD and inside drying chamber, ISGHD at SAH with and without PCM

4.1.6 Effect of mass flow rate (MFR) of air inside SAH and ISGHD system

4.1.6.1 Solar air heating (SAH) system

The corrugated SAH system displayed diverse temperature profiles across different mass flow rates (MFRs). At an MFR of 0.0067 kg/s, the inlet temperature (T_{in}) fluctuated between 24 and 30 °C, while the plate temperature (T_{plate}) ranged from 65 to 110 °C, and the outlet temperature (T_{out}) spanned from 37 to 70 °C. Similarly, at an MFR of 0.012 kg/s, (T_{in}) remained within the 24 to 30 °C range, (T_{plate}) varied from 65 to 103 °C, and (T_{out}) ranged from 36 to 64 °C. At an MFR of 0.018 kg/s, T_{in}, T_{plate}, and T_{out} showed respective ranges of 24 to 30 °C, 59 to 98 °C, and 34 to 61 °C. Finally, at an MFR of 0.024 kg/s, T_{in}, T_{plate}, and T_{out} had temperature ranges of 24 to 30 °C, 65 to

102 °C, and 37 to 72 °C, respectively. These comprehensive temperature profiles highlight the dynamic thermal behaviour of the SAH system at different MFR as shown in Fig. 4.1.10 (a-d).

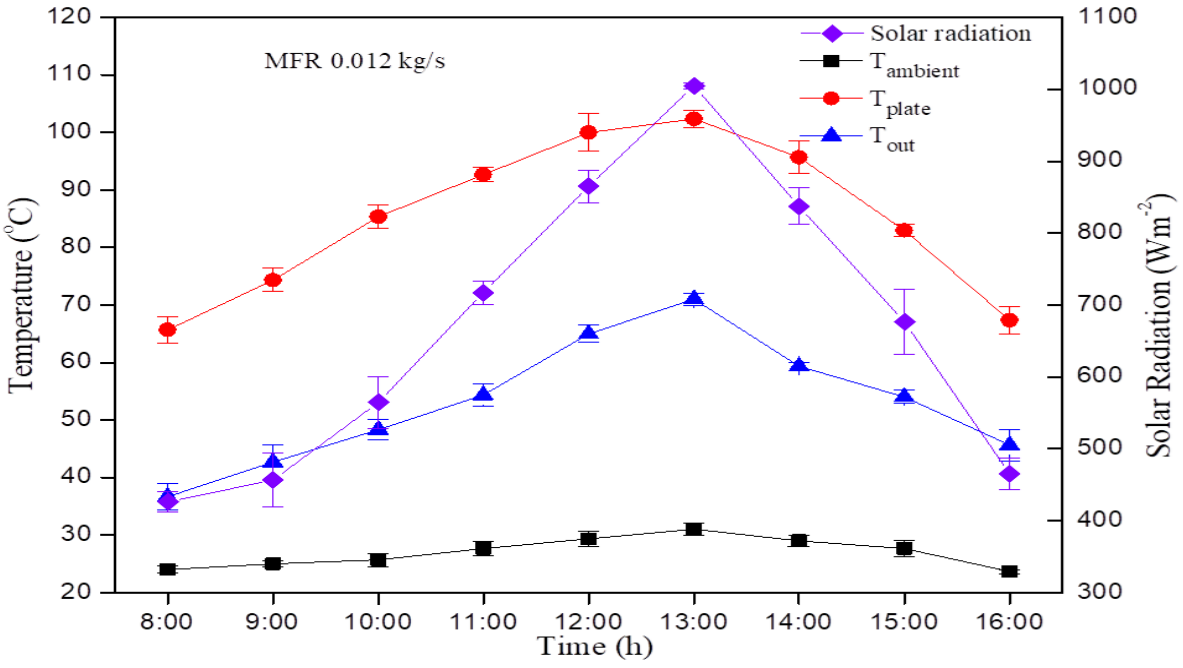

(a)

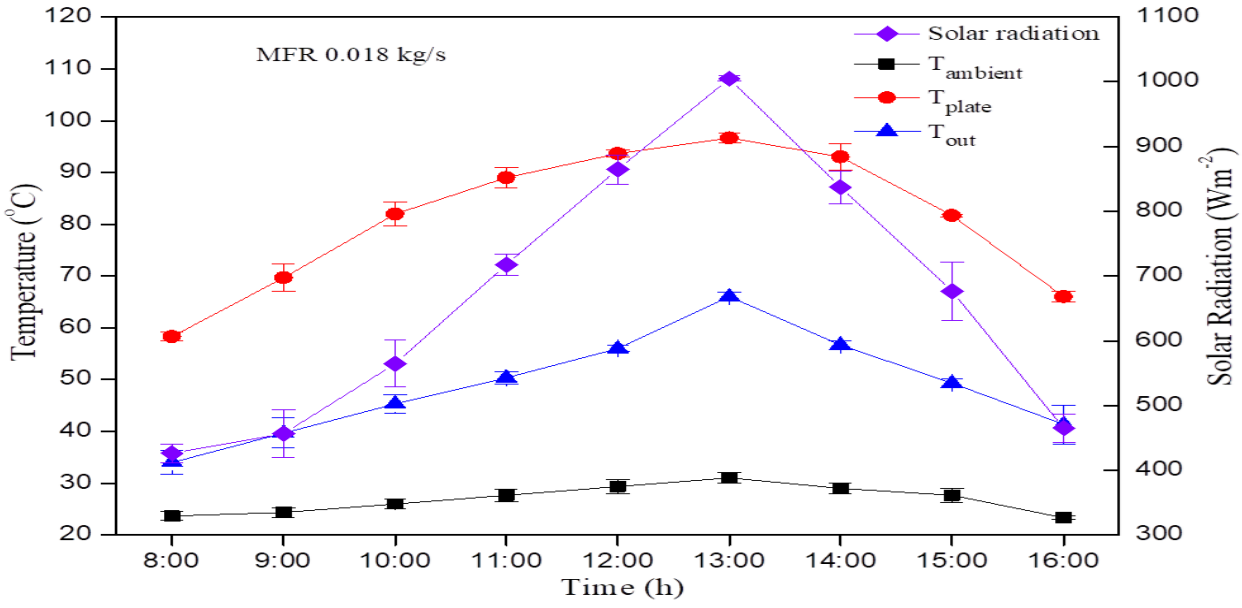

(b)

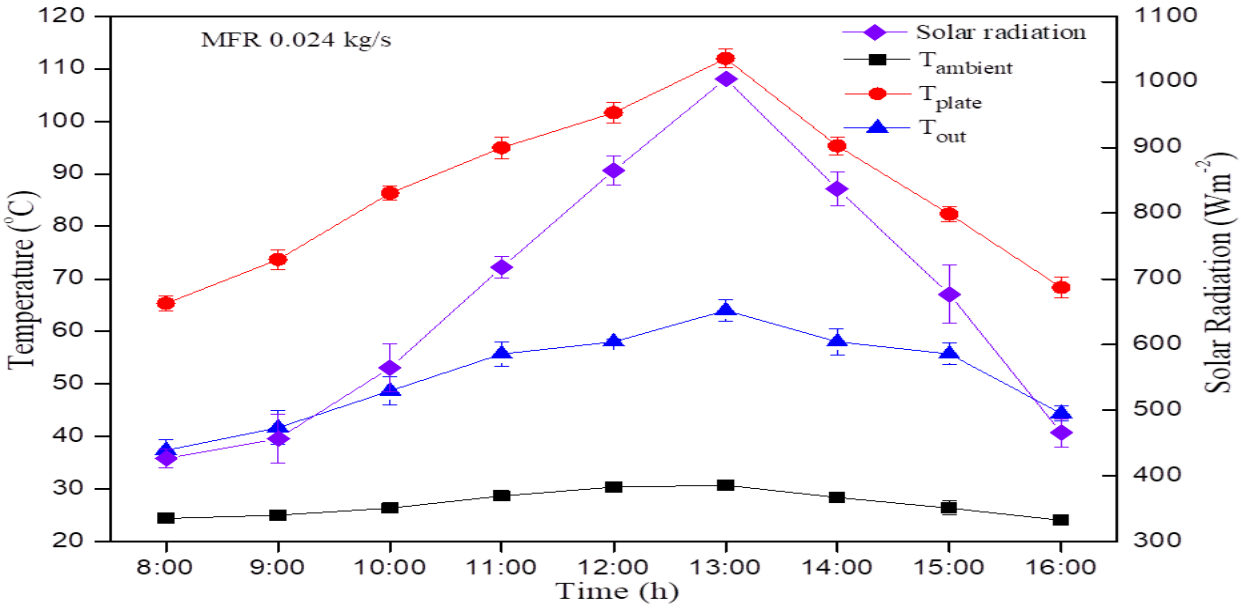

(c)

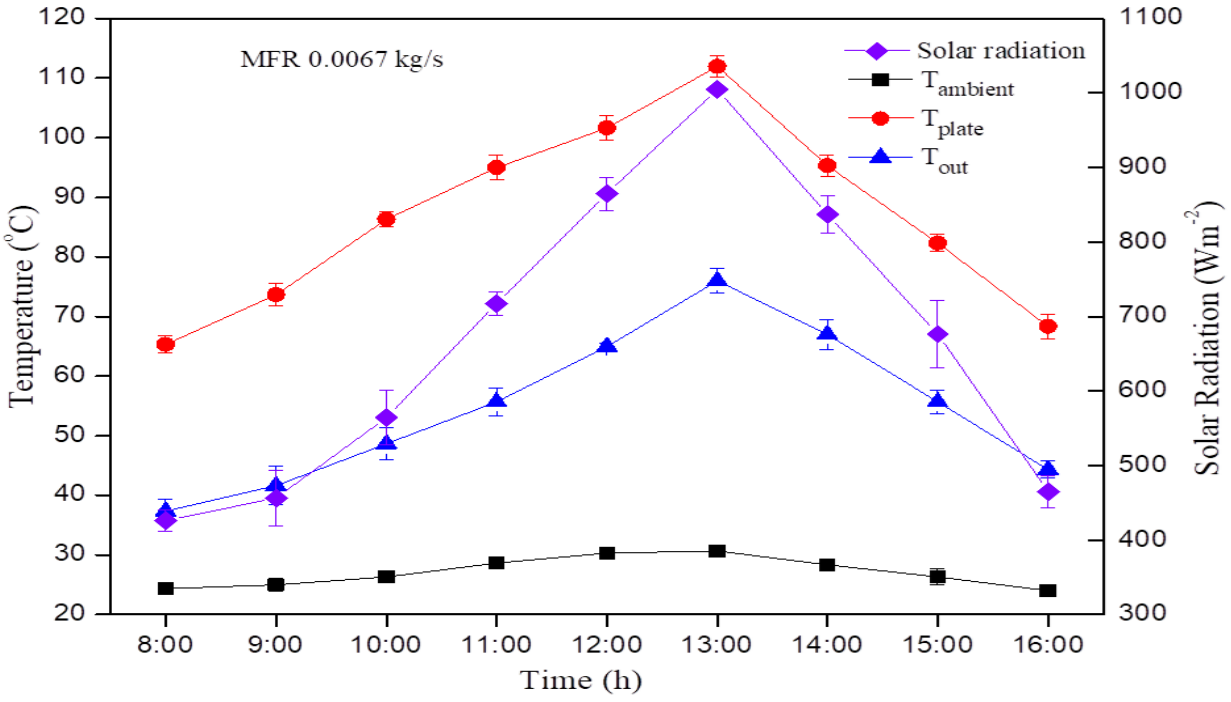

(d)

Fig. 4.1.10 Temperature profile of SAH at different (a)MFR 0.0067 kg/s, (b) 0.012 kg/s, (c) 0.018 kg/s and (d) 0.024 kg/s

The outlet temperature of the corrugated SAH varied with different (MFRs). At a mass flow rate of 0.0067 kg/s, the temperature ranged from 37 to 71 °C. Increasing the mass flow rate to 0.012 kg/s resulted in an outlet temperature range of 35 to 65 °C. Further adjustment to MFR of 0.018 kg/s led to an outlet temperature fluctuating between 32 to 60 °C. Lastly, at a mass flow rate of 0.024 kg/s, the outlet temperature spanned from 31 to 48 °C, as shown in Fig. 4.1.11.

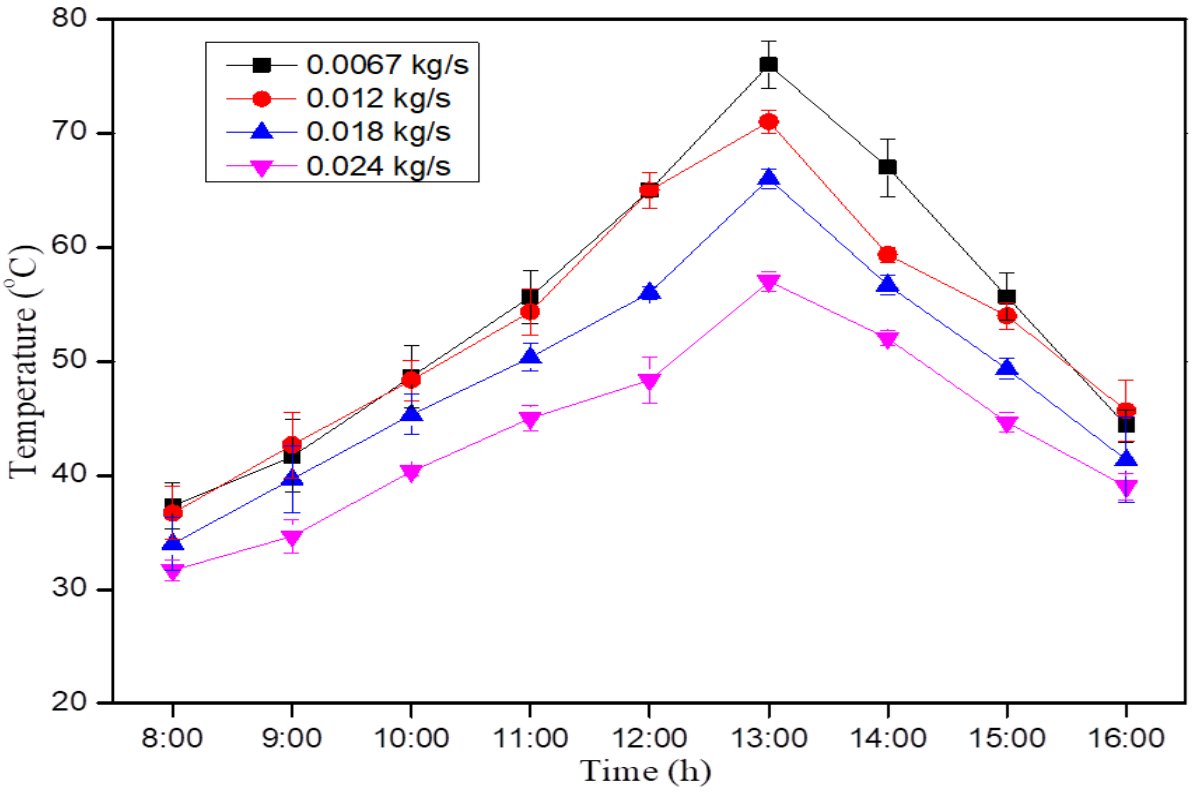

Fig. 4.1.11 SAH output temperature at different MFR at 0.0067 kg/s, 0.012 kg/s ,0.018 kg/s and 0.024 kg/s

4.1.6.2 Integrated solar greenhouse drying (ISGHD) system

The experiment evaluated temperature variations within an ISGHD drying system across different MFRs of air. Temperatures ranged from 33 to 54 °C, 30 to 57 °C, 30 to 59 °C, and 29 to 48 °C for MFRs of 0.012 kg/s, 0.018 kg/s, and 0.024 kg/s, respectively. Highest temperature was observed from 12:00 to 1:00 p.m. Notably, the optimal temperature conditions were observed at an MFR of 0.018 kg/s, indicating superior efficiency and reduced drying time compared to fixed MFR settings. This finding underscores the significance of airflow rate in optimizing drying performance within the ISGHD system, as depicted in (Fig. 4.1.12).

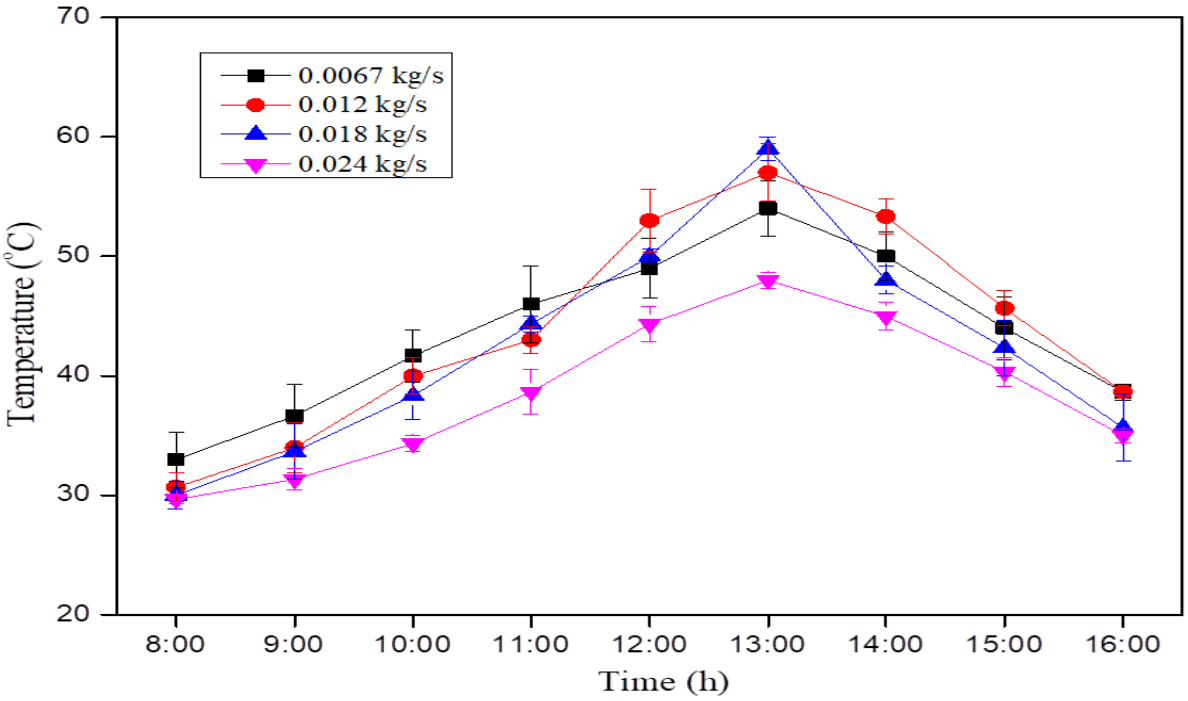

Fig. 4.1.12 Temperature of ISGHD in drying chamber at different MFR

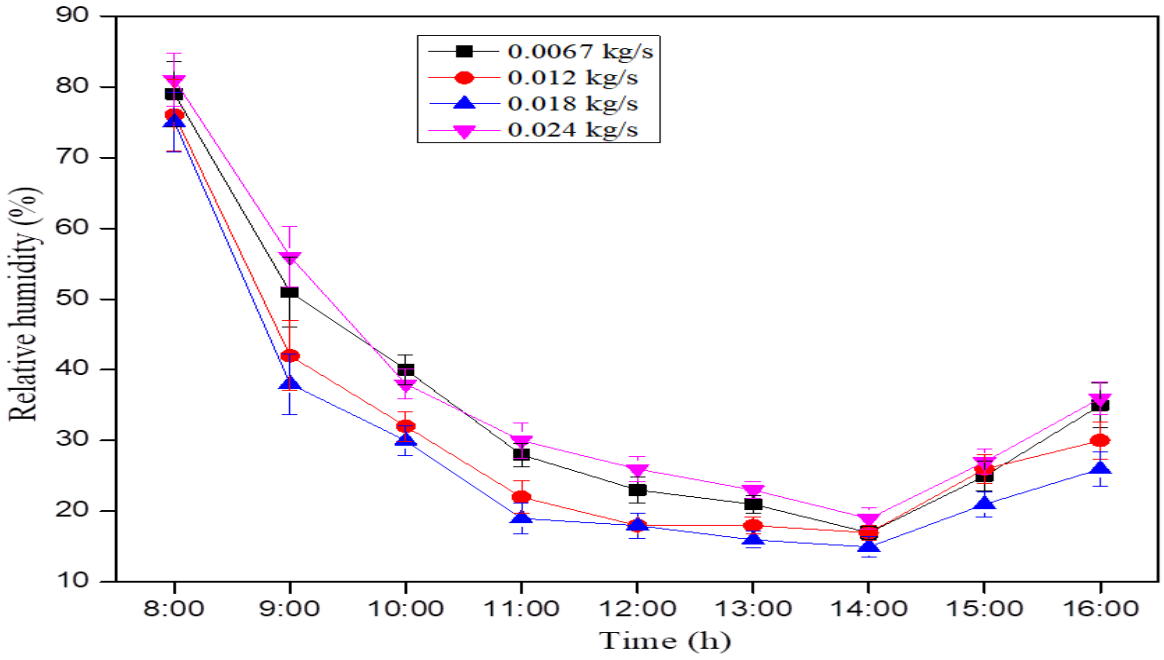

Fig. 4.1.13 Relative humidity of ISGHD in drying chamber at different MFR

And for the relative humidity (RH) levels within the ISGHD drying chamber exhibited significant reductions across different mass flow rates (MFRs). RH decreased from 79% to 18%, 76% to 20%, 75% to 15%, and 81% to 21% for MFRs of 0.012 kg/s, 0.018 kg/s, and 0.024 kg/s, respectively.

Notably, the lowest RH levels were recorded during midday hours, particularly from 12:00 to 1:00 p.m., coinciding with high temperatures inside the drying chamber, as shown in (Fig. 4.1.13). It's observed that as chamber temperature increased, RH automatically decreased. Remarkably, the most optimal RH conditions for drying were observed at an MFR of 0.018 kg/s. Lower RH levels signify improved drying efficiency and reduced drying time, indicating the significance of controlling airflow rates for enhanced drying performance in the ISGHD system.

4.2 Drying characteristics, modelling and quality analysis

4.2.1 Moisture content (MC), moisture ratio (MR) and drying rate (DR)

The study aimed to evaluate the drying characteristics of fresh ginger with an initial moisture content of 86%, employing various slice thicknesses (3.0, 5.0, and 7.0) mm and different drying methods such as open sun drying, OSD (Natural conventional mode), solar greenhouse drying, SGHD (Passive mode), integrated solar greenhouse drying, ISGHD (Active mode) and existing mechanical drying method such as tray drying (TD) and refractance window drying (RWD) for the comparing results. (Fig. 4.2.1) shows the flow chart for different drying methods for ginger drying.

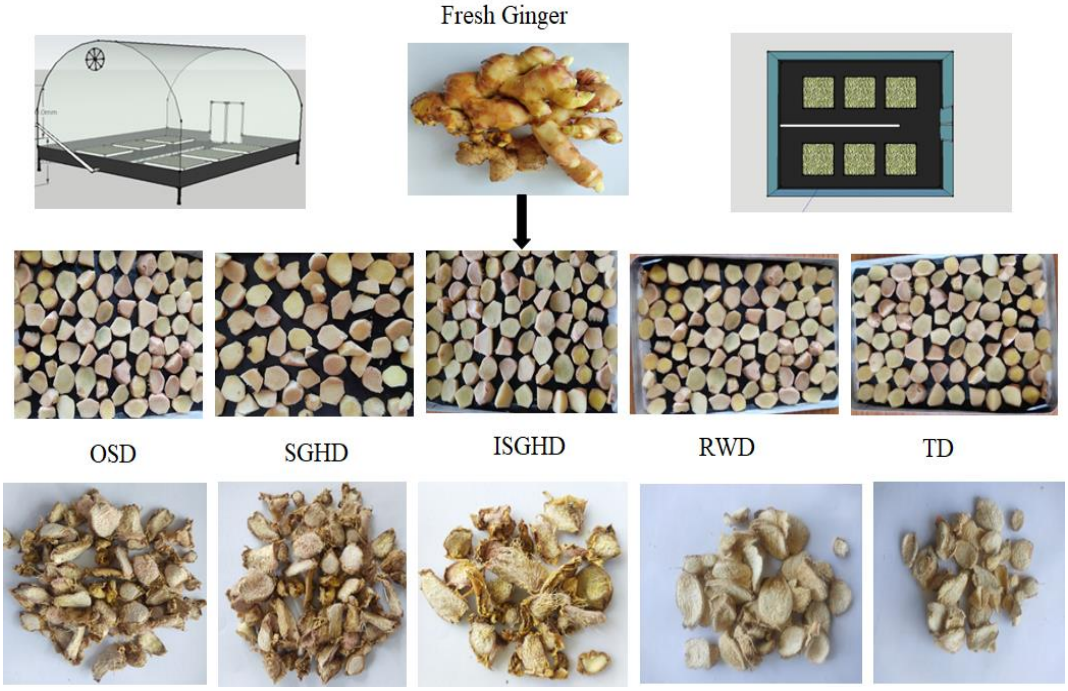

Fig. 4.2.1 Flowchart for drying of ginger slices at different drying methods

Drying characteristics such as the deviation of MC, MR, and DR were observed in the experiment for 3.0 mm slices of ginger. Initially, the moisture content of fresh ginger was 84%, which was reduced to a safe level of 10% using different drying methods. The drying times were 54 h, 50 h, 29 h, 17 h, and 15 h in OSD, SGHD, ISGHD, TD, and RWD, respectively as shown in (Fig. 4.2.2). Moisture content decreases if temperature increases. Here, we found that an integrated solar greenhouse drying system (ISGHD, Active mode), which is based on solar radiation energy, will take less time to dry ginger as compared to OSD (natural) and SGHD (Passive) and very near close to existing mechanical drying method TD and RWD. The potential of ISGHD as an effective and energy-efficient drying solution for ginger. This is because greenhouse drying systems are equipped with a solar battery backup, which is charged by a PV panel. The system is to operate the DC blower and exhaust fan for 4-6 hours, even when there is no sunshine. The DC blower supplies air through SAH, and the DC exhaust removes the air inside the dryer regularly to prevent moisture accumulation inside the dryer. As a result, the humidity and airflow can be controlled more accurately, leading to a faster drying process. The graph of moisture content versus drying time for ginger slices is depicted in Fig. 4.2.2, indicating that as drying time increases, moisture content continuously decreases.

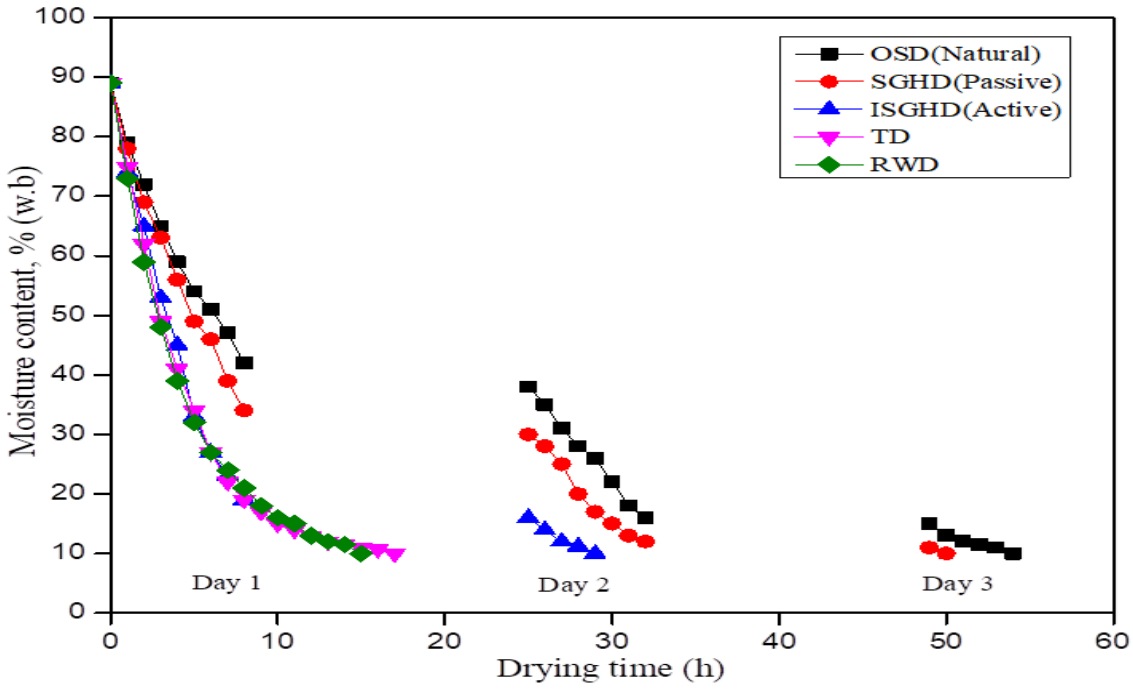

Fig. 4.2.2 Moisture content vs drying time curve for 3.0 mm thickness of ginger slices

The MR decreased from 1.0 to 0.10 when drying 3.0 mm ginger slices in the ISGHD method as compared to OSD and SGHD, which are dependent on solar drying while near close to the existing mechanical drying method. However, ISGHD showed the highest moisture ratio among solar drying methods, closely comparable to mechanical drying (TD and RWD). Higher airflow rates and temperatures led to a greater moisture ratio due to increased effective moisture diffusion during drying, as depicted in (Fig. 4.2.3).

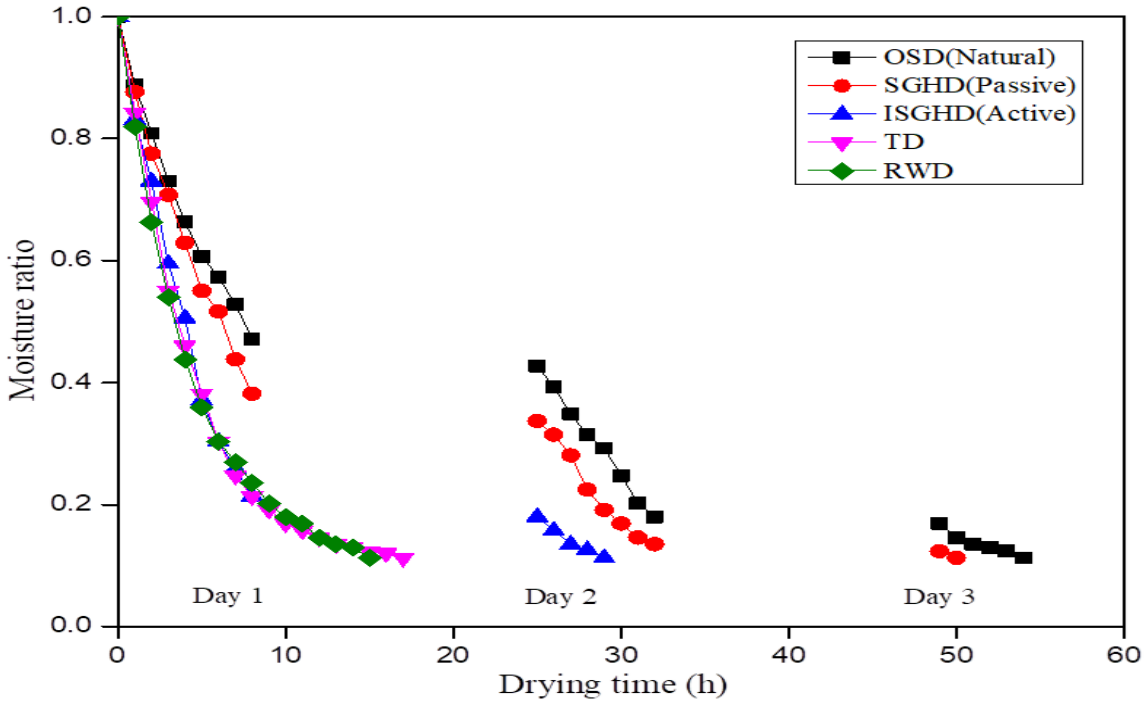

Fig. 4.2.3 Moisture ratio vs drying time curve for 3.0 mm thickness of ginger slices

The graph of drying rate versus drying time in (Fig. 4.2.4) demonstrates a continual decline in the sample's drying rate over time. Among the methods tested, OSD, SGHD, ISGHD, TD, and RWD achieved maximum drying rates of 1.4, 1.7, 2.3, 2.1, and 2.5 kg water/kg dry solid*h, respectively. Notably, ISGHD exhibited the highest drying rate among the solar drying methods. The rapid initial increase in drying rate is due to free moisture on the surface. Additionally, increasing airflow rate and temperature resulted in higher drying rates.

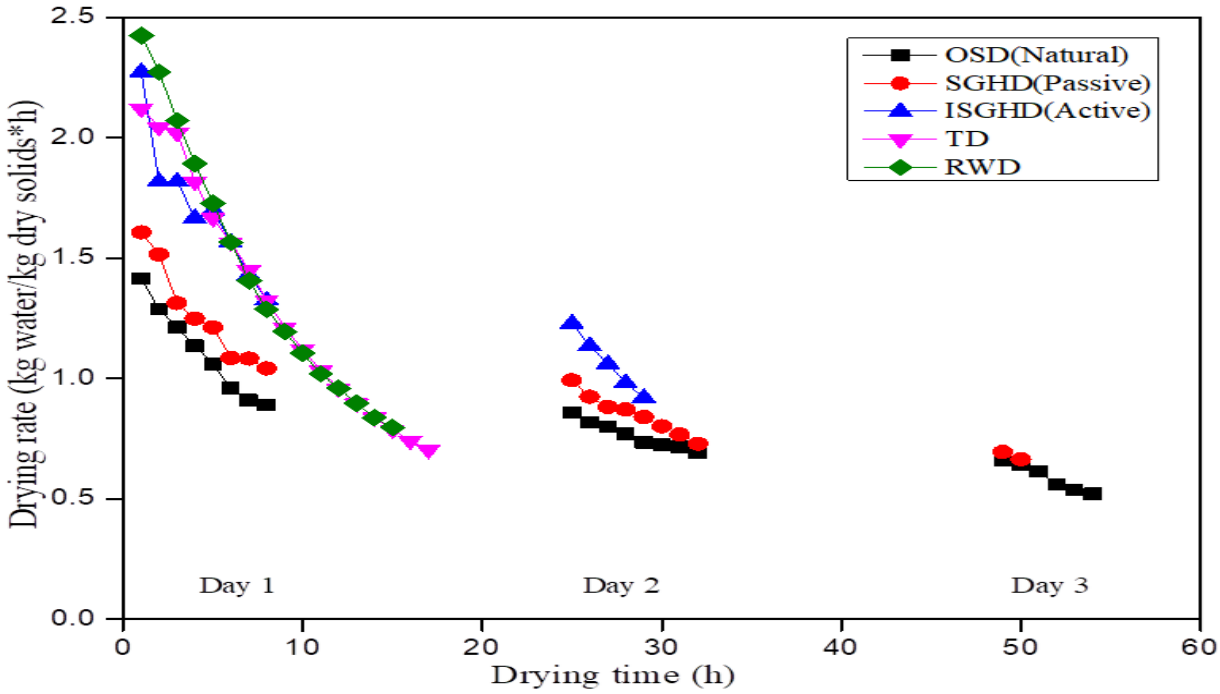

Fig. 4.2.4 Drying rate vs drying time curve for 3.0 mm thickness of ginger slices

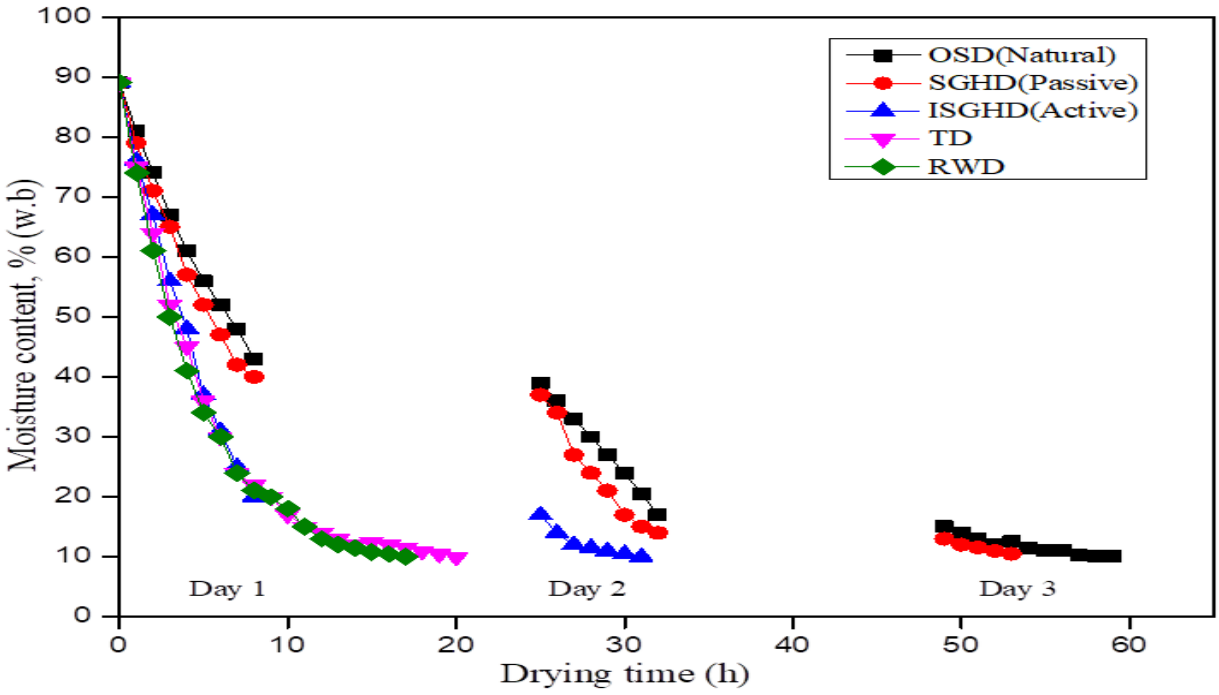

Fig. 4.2.5 Moisture content vs drying time curve for 5.0 mm thickness of ginger slices

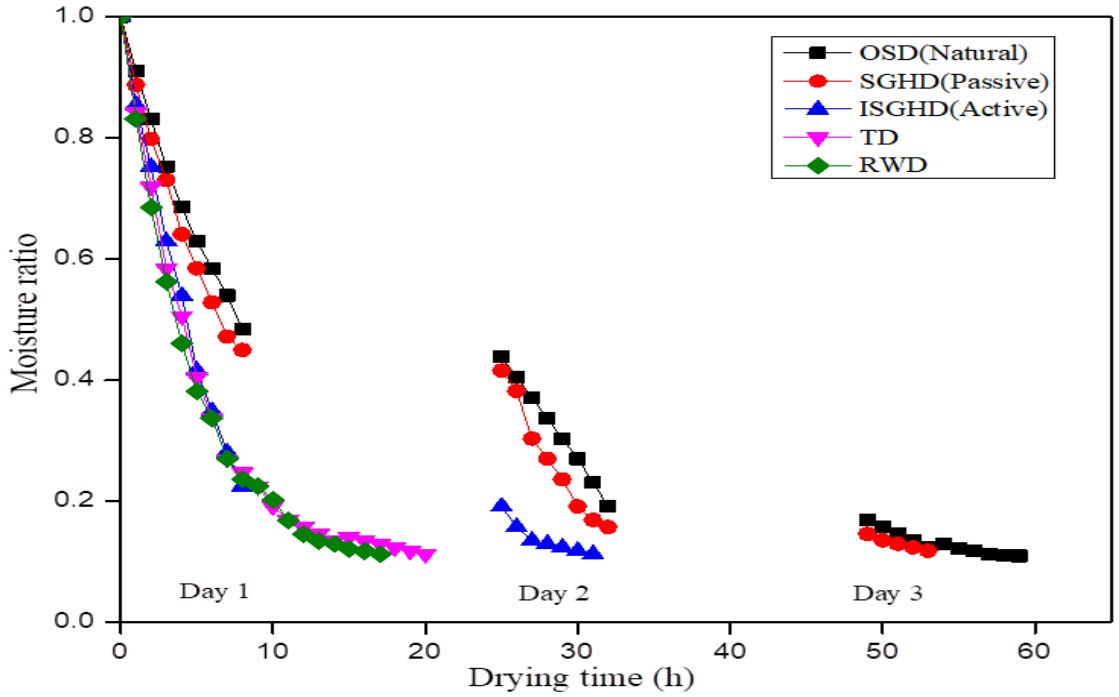

Fig. 4.2. 6 Moisture ratio vs drying time curve for 5.0 mm thickness of ginger slices

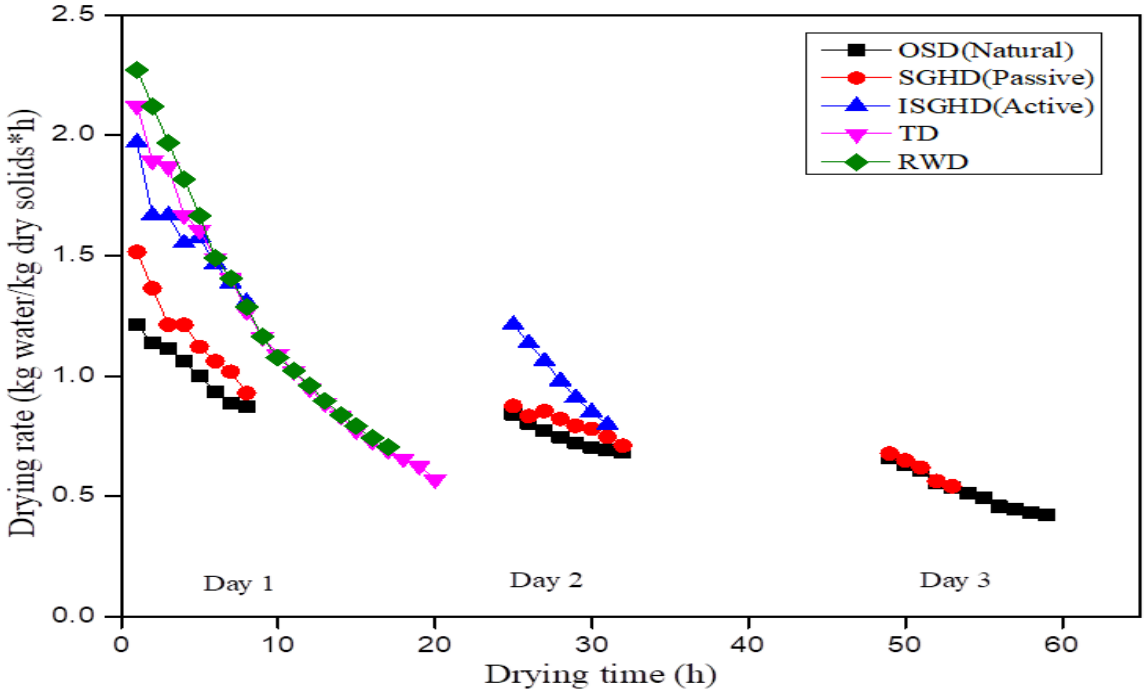

Fig. 4.2.7 Drying rate vs drying time curve for 5.0 mm thickness of ginger slices

Similarly, the moisture content for 5.0 mm thickness ginger slices is represented in (Fig. 4.2.5), where the drying times were 59 h, 57 h, 31 h, 20 h, and 18 h in OSD, SGHD, ISGHD, TD, and

RWD respectively. (Fig. 4.2.6) depicts the moisture ratio for different drying methods, revealing that the moisture ratio decreases as drying time increases. Furthermore, the drying rate diminishes with longer ginger drying times, as shown in (Fig. 4.2.7).

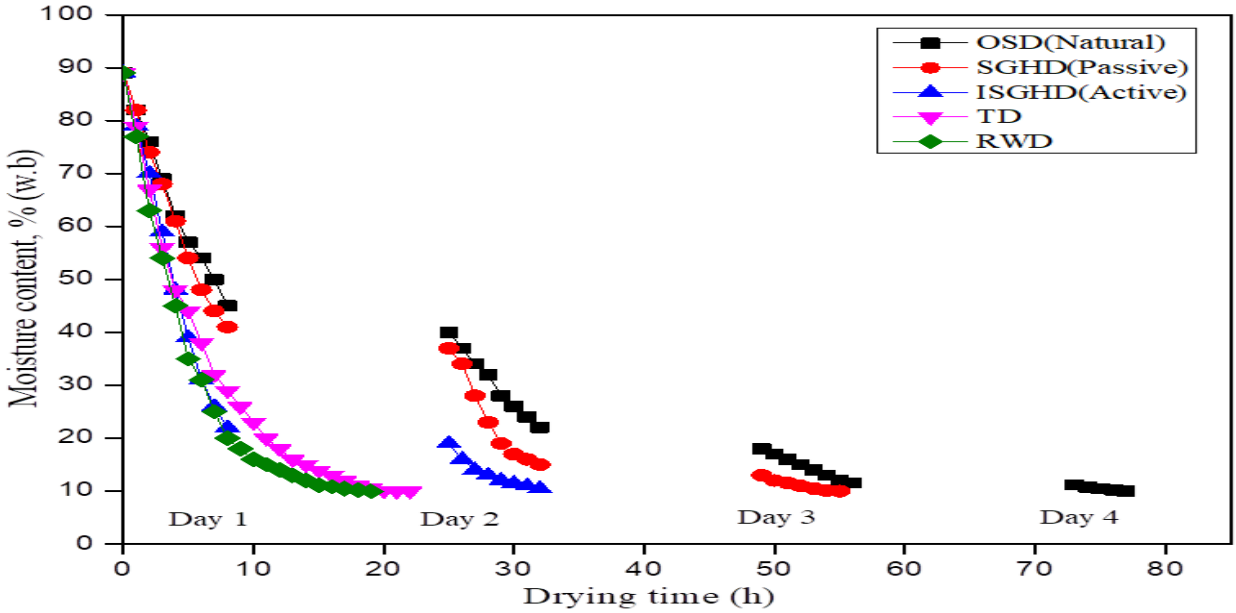

Fig. 4.2.8 Moisture content vs drying time curve for 7.0 mm thickness of ginger slices

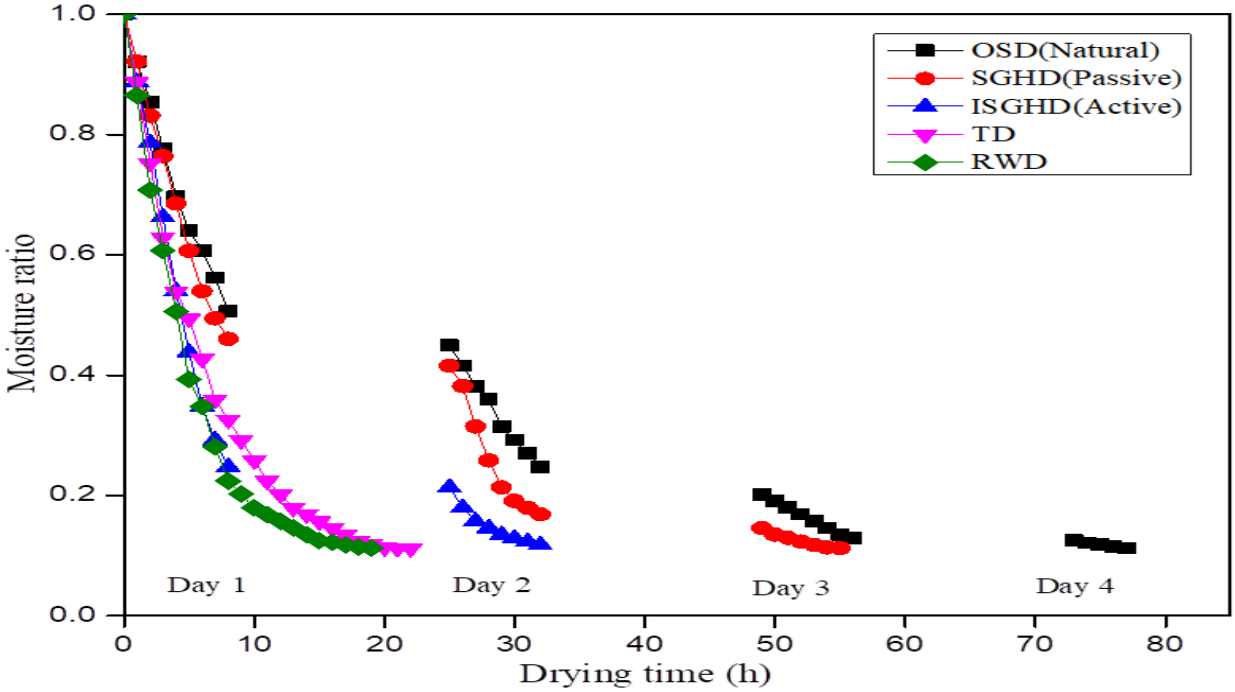

Fig. 4.2.9 Moisture ratio vs drying time curve for 7.0 mm thickness of ginger slices

Similarly, the moisture content for 7.0 mm thickness ginger slices is represented in (Fig. 4.2.8), where the drying times were 77 h, 54 h, 32 h, 22 h, and 19 h in OSD, SGHD, ISGHD, TD, and RWD respectively. (Fig. 4.2.9) depicts the moisture ratio for different drying methods, revealing that the moisture ratio decreases as drying time increases. Furthermore, the drying rate diminishes with longer ginger drying times, as shown in (Fig. 4.2.10).

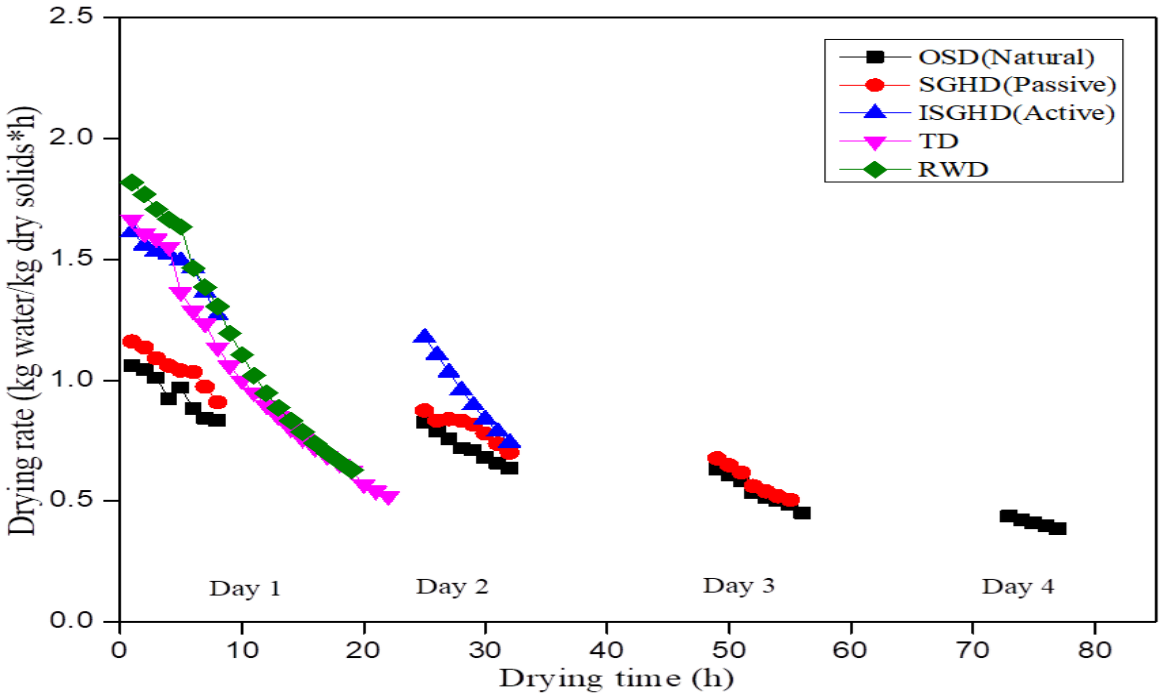

Fig. 4.2.10 Drying rate vs drying time curve for 7.0 mm thickness of ginger slices

The experiment revealed that achieving the safe moisture content level of 10% for fresh ginger slices took less time in the case of ISGHD (SAH with PCM) compared to ISGHD (SAH without PCM), represented in (Fig. 4.2.11). This finding underscores the effectiveness of incorporating PCM into the solar heating system for improved drying efficiency. During periods of off-sunshine hours or nighttime, the temperature and relative humidity (RH) inside the dryer were maintained for at least 3-4 hours with the assistance of SAH with PCM. The integration of PCM proved to be highly beneficial for ensuring efficient drying and reducing the overall time required for ginger drying. By harnessing solar energy and utilizing PCM, the system could effectively regulate the drying environment, optimizing conditions for the drying process and enhancing its effectiveness.

As a result, the use of PCM contributed significantly to the efficiency and efficacy of the drying operation, facilitating faster and more effective ginger drying.

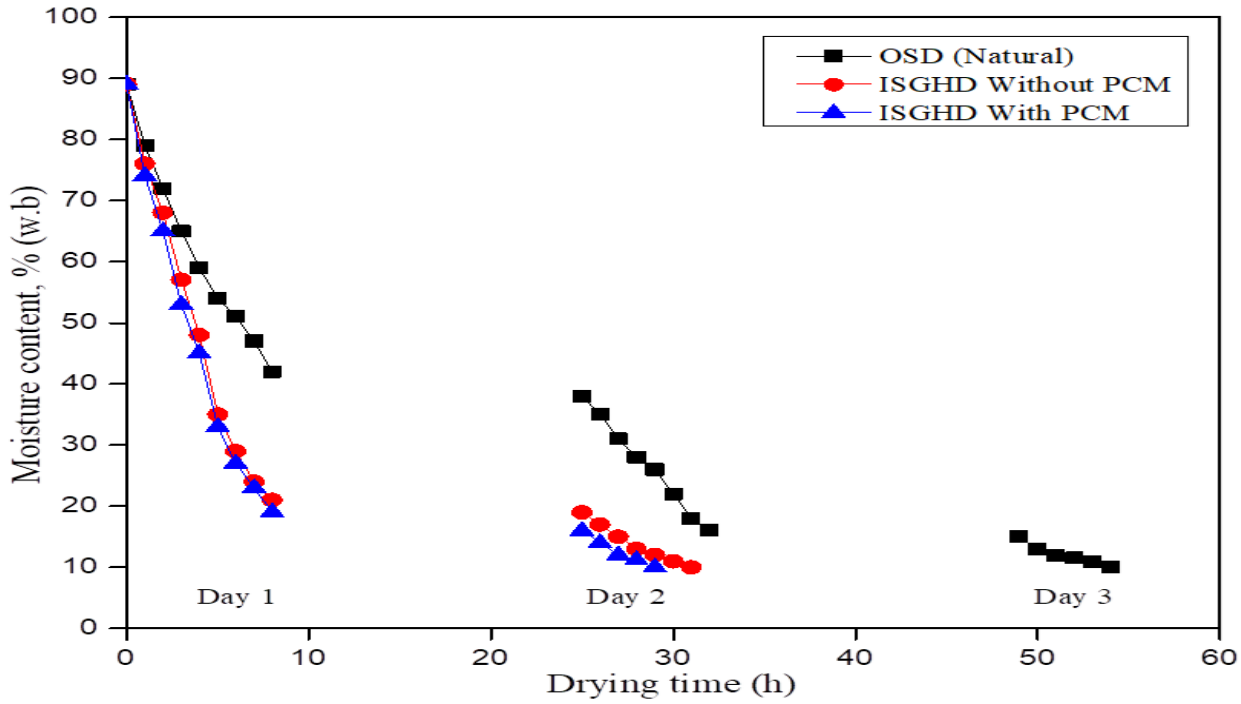

Fig. 4.2.11 Effect of SAH (with or without PCM) in drying of ginger slices

4.2.2 Moisture diffusivity

Effective moisture diffusivity (D_{eff}) is essential for understanding moisture transport in food materials during drying, especially in the falling rate periods. Fig. 4.2.12 shows D_{eff} for ginger slices of different thicknesses dried using various methods. ISGHD notably exhibits higher D_{eff}, possibly due to variances in moisture vapor pressure and increased mass transfer at higher airflow rates (0.018 kg/s) during drying.

4.2.3 Drying kinetics model

Ten drying models were used to investigate the drying kinetics for ginger slices, and nonlinear regression analysis was performed using MATLAB R2018b. Drying kinetics models were customized according to the MR values of ginger slices dried using various drying methods. (Fig. 4.2.13(a-d)), illustrates the comparison between predicted and experimental MR using different drying models for (a) OSD, (b) ISGHD, (c) TD, and (d) RWD.

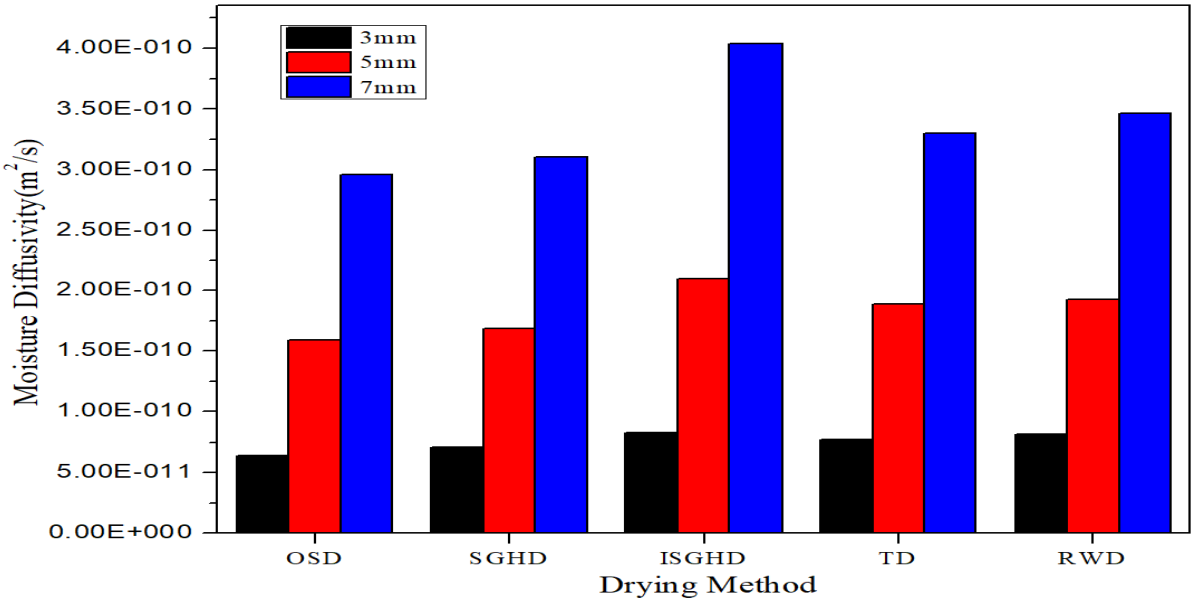

Fig. 4.2.12 Moisture diffusivity of ginger slices by using different drying methods

A summary of the statistical indicators of goodness of fit for all the ten drying models alongside their coefficients is presented in **Appendix-A**. A higher R^2 and a lower χ^2 value are considered strong indicators of a good fit. The analysis reveals that all selected models exhibit a satisfactory fit within the valid range of goodness. However, among them, the Page model, logarithmic model, and Newton model stand out as the best-fitted, showcasing superior performance for the dried ginger slices. This finding underscores the effectiveness of these models in accurately representing the drying process and highlights their potential for practical application in optimizing drying operations. A discussion on the best three drying models is presented in following sub-sections.

4.2.3.1 Page model

For the drying kinetics of ginger slices, it was found that the Page model provided the best fit among all ten models. We compared the drying methods for ginger slices using the best-fitted model. The Page model yielded superior results in ISGHD (R^2=0.99998 and χ^2=0.00016), followed by RWD (R^2=0.99978 and χ^2=0.00013), TD (R^2=0.99936 and χ^2=0.00024), and OSD (R^2=0.99978 and χ^2=0.00021). A higher R^2 and a lower χ^2 value are considered strong indicators of a good fit. Fig. 4.2.14 represents the experimental and predicted moisture ratio values for ginger drying using the Page model.

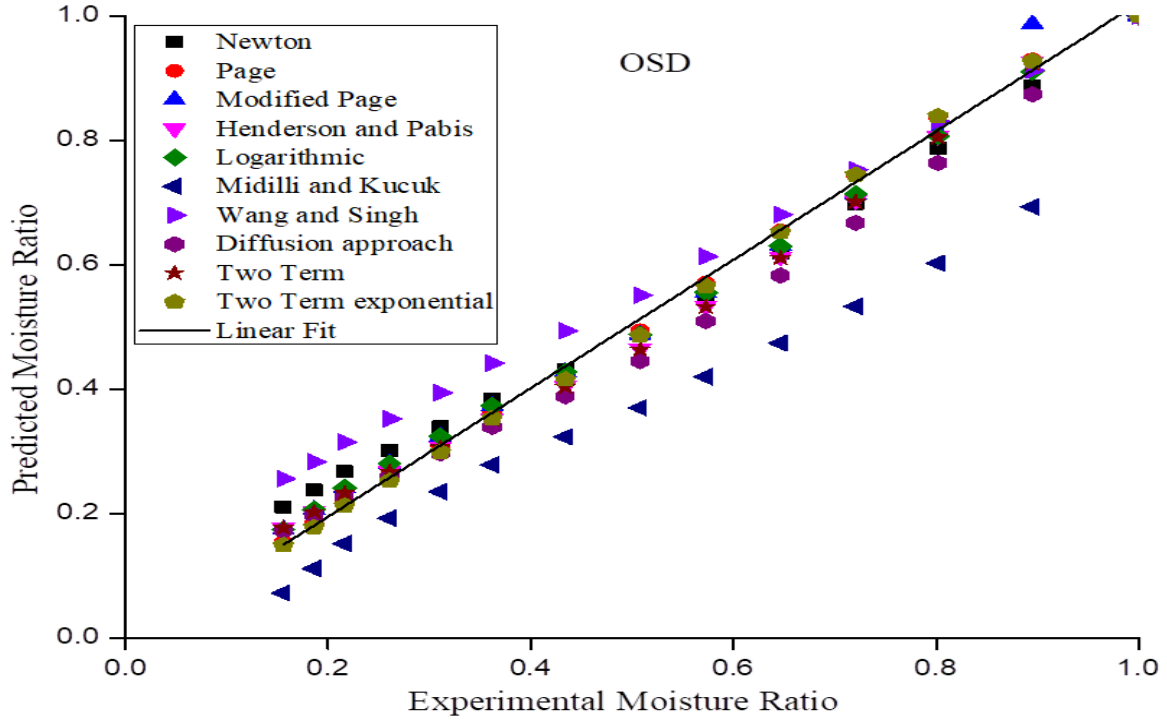
OSD
Newton
Page
Modified Page
Henderson and Pabis
Logarithmic
Midilli and Kucuk
Wang and Singh
Diffusion approach
Two Term
Two Term exponential
Linear Fit
Predicted Moisture Ratio
Experimental Moisture Ratio
0.0
0.2
0.4
0.6
0.8
1.0

(a)

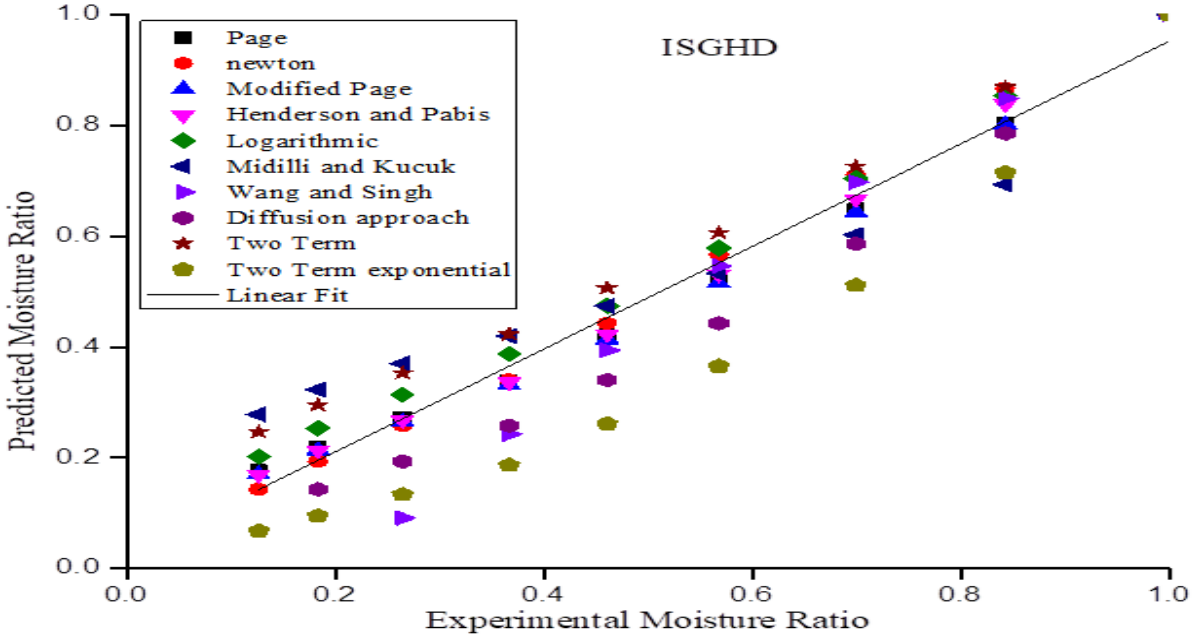
ISGHD
Page
newton
Modified Page
Henderson and Pabis
Logarithmic
Midilli and Kucuk
Wang and Singh
Diffusion approach
Two Term
Two Term exponential
Linear Fit
Predicted Moisture Ratio
Experimental Moisture Ratio
0.0
0.2
0.4
0.6
0.8
1.0

(b)

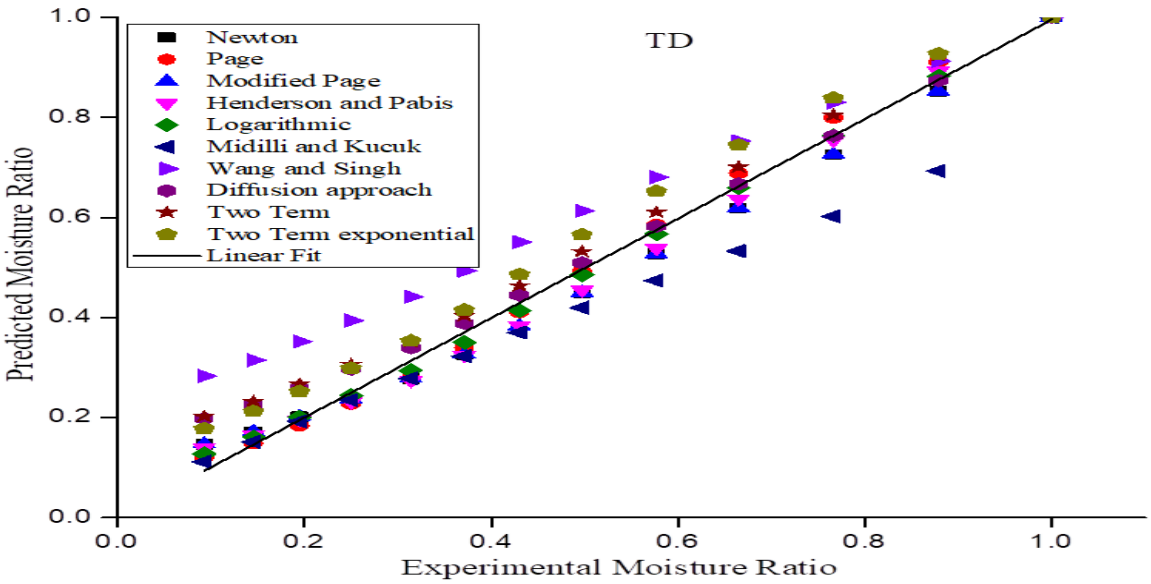

(c)

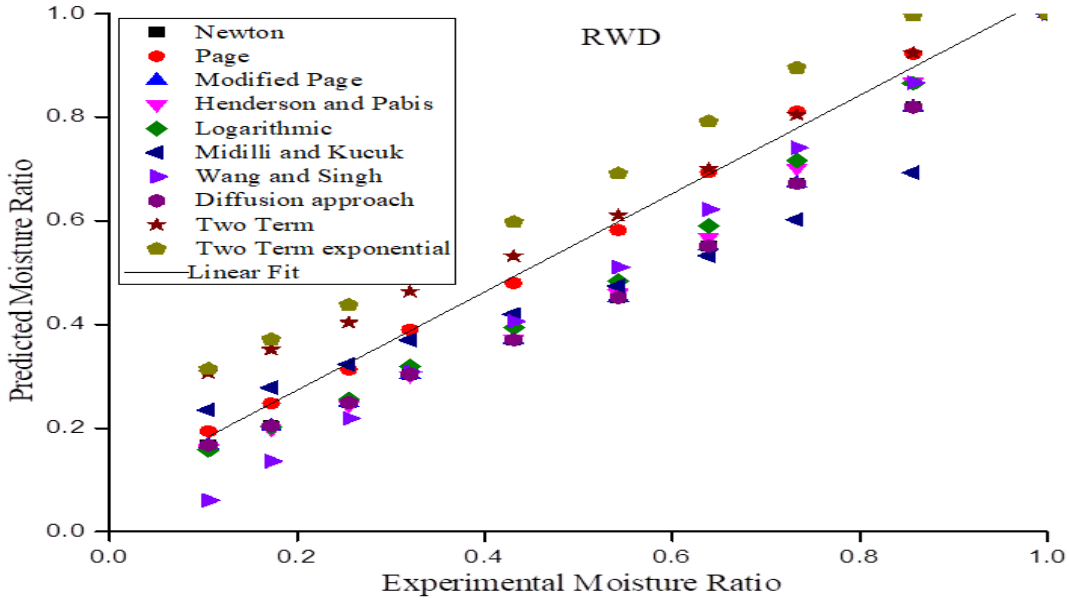

(d)

Fig. 4.2.13 Moisture ratio of predicted and experimental by using different drying models for (a) OSD, (b) ISGHD, (c) TD, and (d) RWD

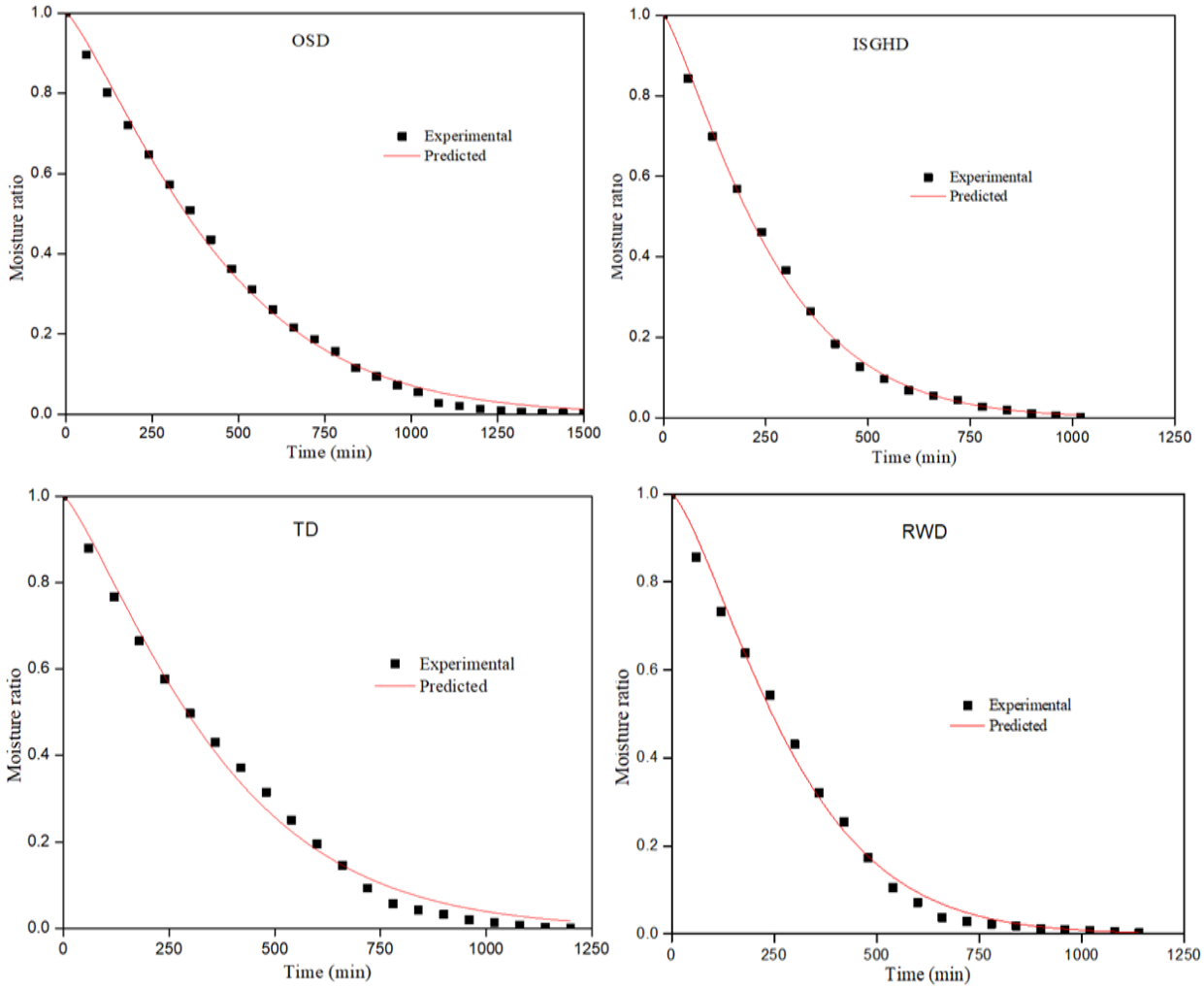

Fig. 4.2.14 Experimental and predicted moisture ratio values for ginger drying using the Page model

4.2.3.2 Logarithmic model

The logarithmic model yielded superior results in ISGHD (R^2=0.99987 and χ^2=0.00032), followed by RWD (R^2=0.99912 and χ^2=0.00025), TD (R^2=0.99891and χ^2=0.00041), and OSD (R^2=0.99923 and χ^2=0.00230). Fig. 4.2.15 represents the experimental and predicted moisture ratio values of ginger drying for the logarithmic model.

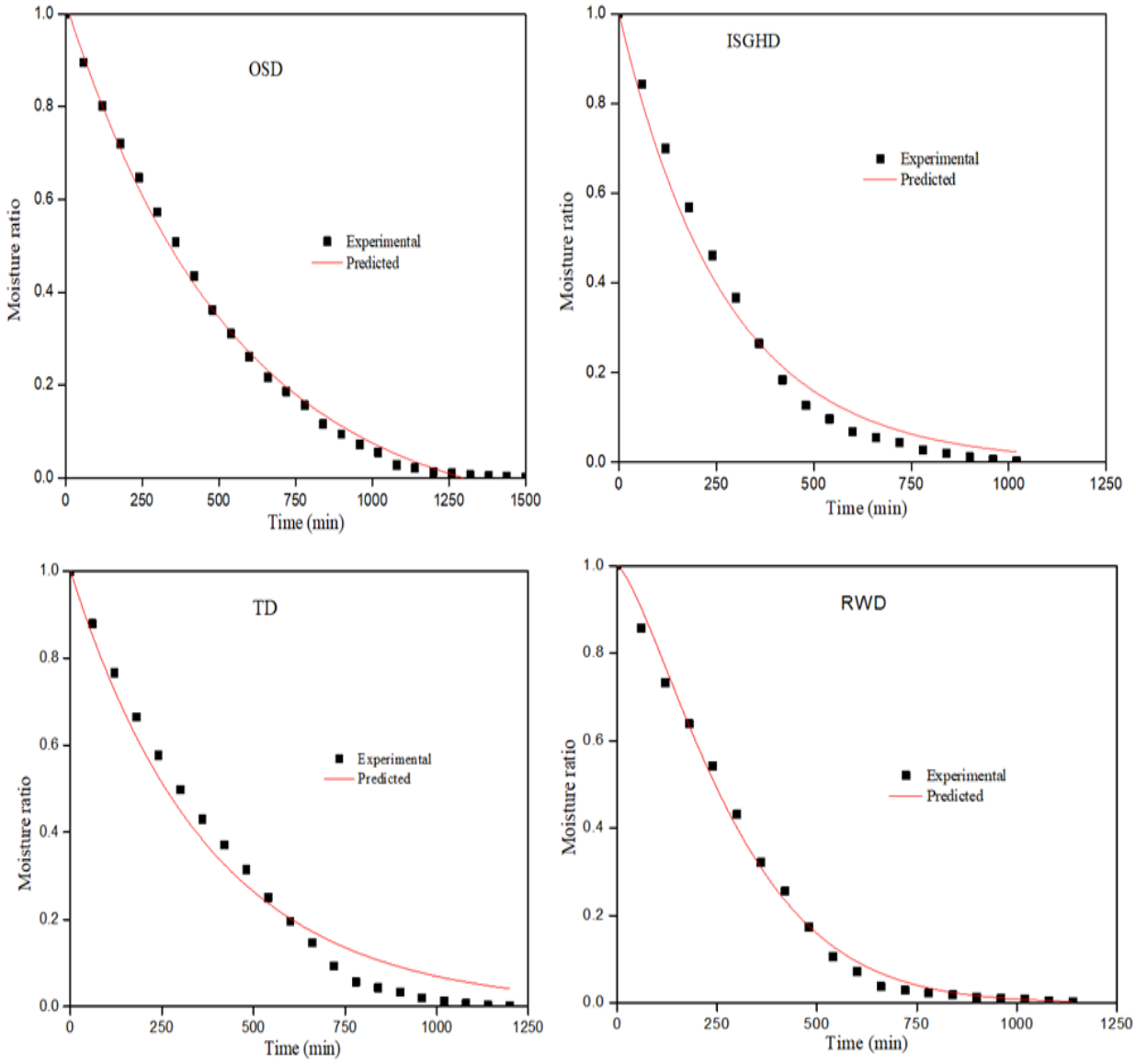

Fig. 4.2. 15 Experimental and predicted moisture ratio value of ginger drying for logarithmic model

4.2.3.3 Newton Model

The Newton model yielded superior results in ISGHD (R^2=0.99447and χ^2=0.00046), followed by RWD (R^2=0.99842and χ^2=0.00097), TD (R^2=0.99684 and χ^2=0.00056), and OSD (R^2=0.98422 and χ^2=0.00125). (Fig. 4.2.16) represents the experimental and predicted moisture ratio values of ginger drying for the Newton model.

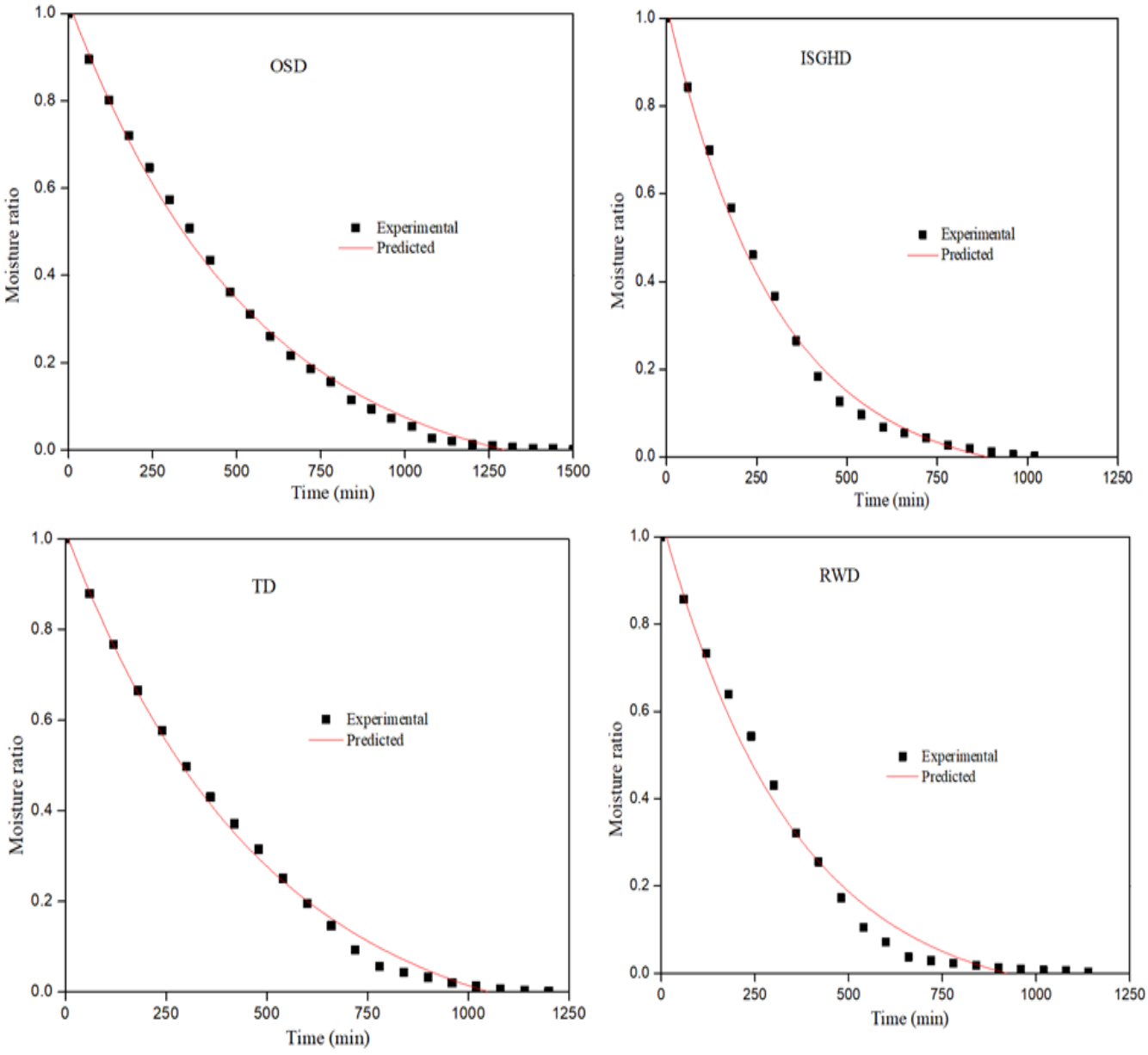

Fig. 4.2.16 Experimental and predicted moisture ratio value of ginger drying for Newton model

4.2.4 ANN

Artificial neural network (ANN) was also used to predict the kinetics of ginger drying. The NN toolbox from MATLAB 2018b programme was used to fit the MC, MR, and DR values as output parameters against the drying time (h), solar radiation (Wm^{-2}), drying air temperature (°C), airflow (kg/s), and relative humidity (%) values as input variables.

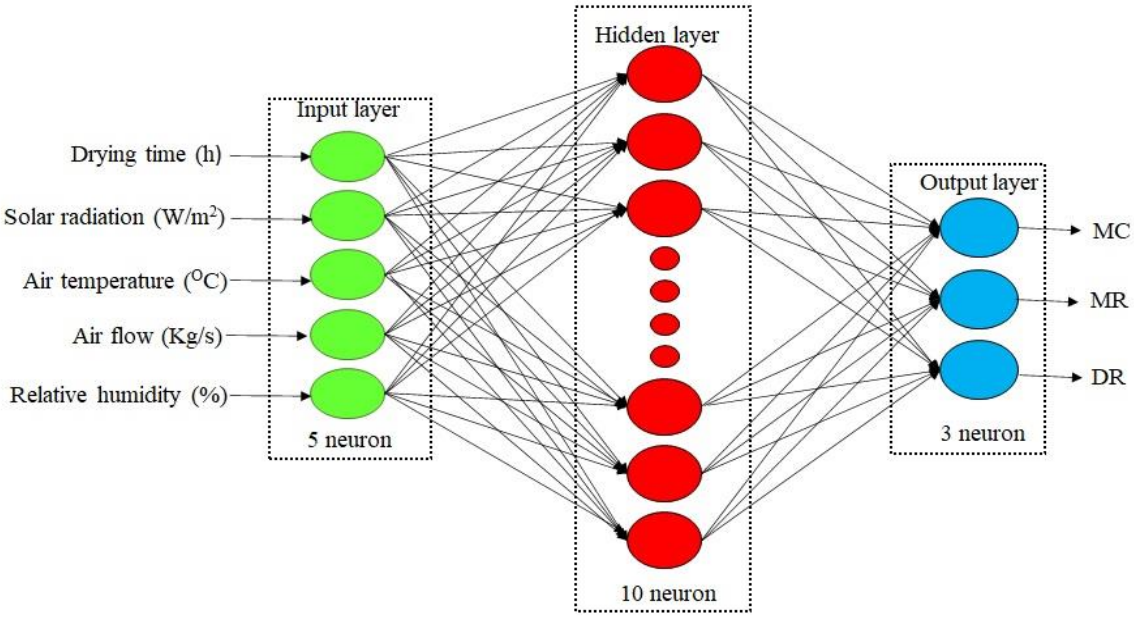

Fig. 4.2.17 ANN structure

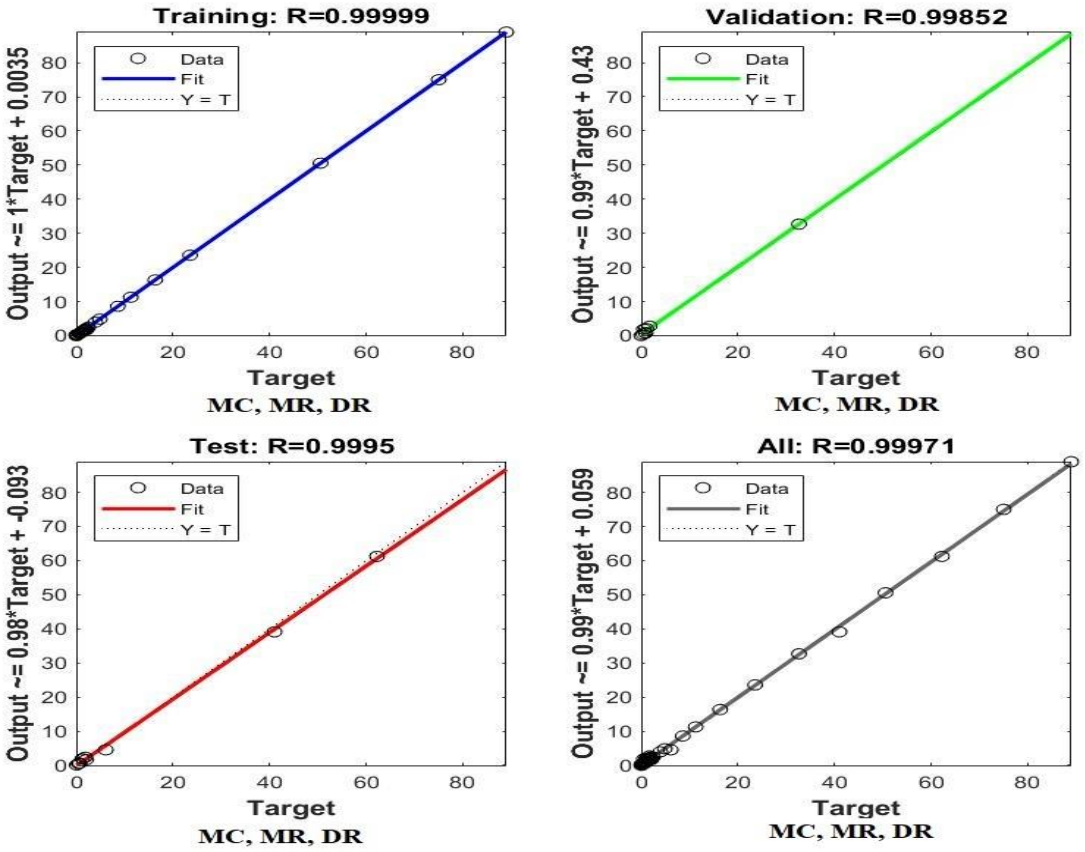

Fig. 4.2.18 ANN regression graph of MC, MR, and DR for ISGHD method

The developed ANN structure had five and three neurons, respectively, for the input and output layers, and the 5-10-3 architecture was chosen for the study of ginger drying. The selected ANN resulted in an R^2 value of more than 0.99971. As shown in (Fig. 4.2.17), the ANN predicted and experimental data were in excellent agreement, with a low relative deviation value. (Fig. 4.2.18) shows the validation of experimental and predicted data of ginger drying, showing good agreement in MC, MR, and DR, as reported in previous studies [30].

4.2.5 Rehydration ratio (RR)

RR is a key quality indicator of the dried ginger product, with a higher value indicating better quality. (Fig. 4.2.19) presents the rehydration values for dried ginger. The ISGHD drying method demonstrated highest rehydration ratio at 4.2±0.29, followed by the RWD, TD, SGHD and OSD methods with a value of 3.9±0.21, 3.7±0.19, 3.4±0.33 and 3.3±0.34 respectively. The sample with the maximum rehydration ratio of 4.2 was found in the ISGHD system because integrated solar greenhouse drying (ISGHD) provides a controlled environment with optimized temperature, humidity, and airflow, resulting in a higher rehydration ratio, as reported in previous studies for ginger [27]. Additionally, analysis of variance and Turkey's test, determined significant differences ($p \leq 0.05$) among variables of different drying methods.

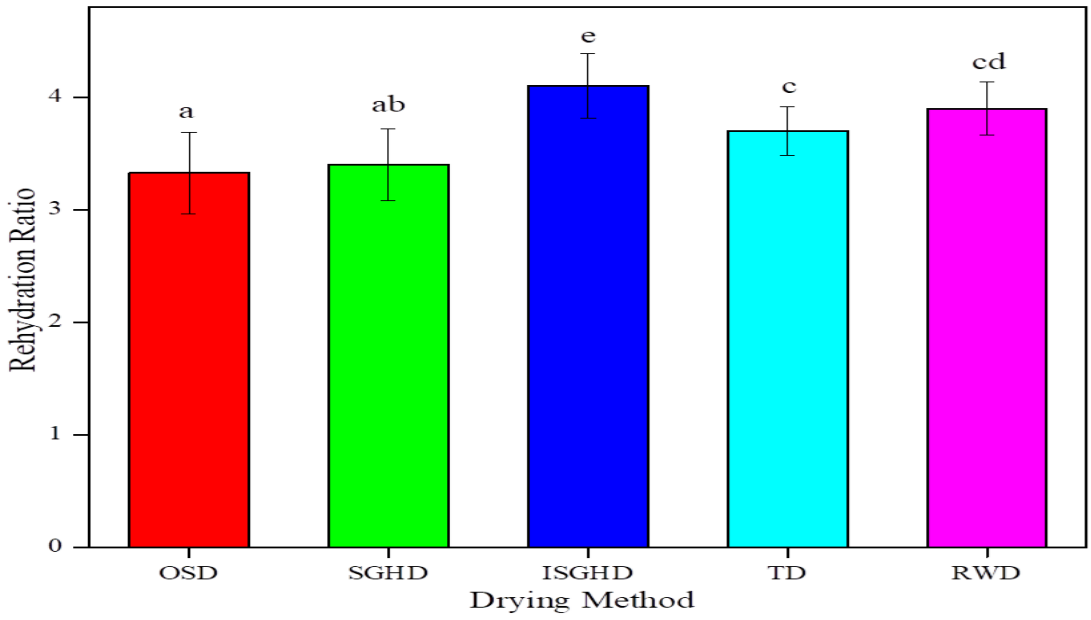

Fig. 4.2.19 Rehydration ratio of ginger slices by using different drying methods, with different letters (a–e) indicating significant differences ($p < 0.05$)

4.2.6 Shrinkage Ratio

Among the evaluated drying methods, the ISGHD drying method exhibited the lowest shrinkage percentage at 57±3.2 %, followed by RWD at 58±2.5 %, SGHD at 64±2.8 %, TD at 67±2.0 %, and OSD with 70±3.6 %. This highlights ISGHD's superior ability to minimize shrinkage compared to the other methods, making it a favourable choice for preserving the integrity of the dried product. The shrinkage ratio values of ginger drying are shown in (Fig. 4.2.20). Additionally, analysis of variance and Turkey's test, determined significant differences ($p \leq 0.05$) among variables of different drying methods.

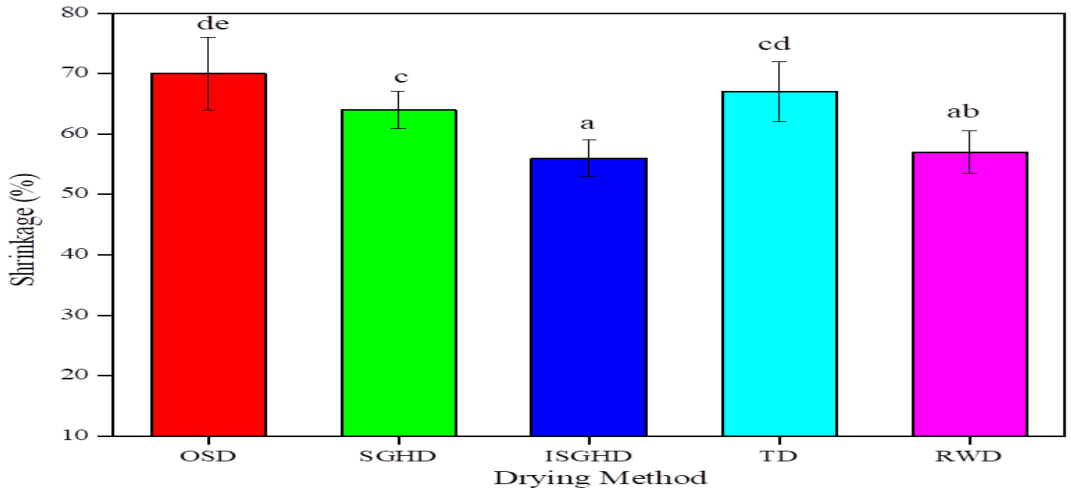

Fig. 4.2.20 Shrinkage ratio of ginger slices for different drying methods, with different letters (a–e) indicating significant differences ($p < 0.05$)

4.2.7 Texture

The crushing strength of dried ginger from all drying techniques is displayed in (Fig.4.2.21). The texture property, specifically hardness, of dried ginger exhibited varying peak force values across different drying methods. The ISGHD drying method demonstrated the lowest peak force at 1233±24 g, followed by RWD with 1428±33 g, TD with 1527±17 g, SGHD with 1560±27 g, and OSD with 1661±30 g. ISGHD ensures thorough drying of ginger slices, allowing fibrous bonds within the structure to break easily, as similar result found in previous studied [27,85]. This makes the slices more brittle and less resistant to crushing, requiring less force. The observed reduction in crushing force highlights ISGHD's effectiveness in producing ginger slices with superior texture, appealing to consumers and food processors alike.

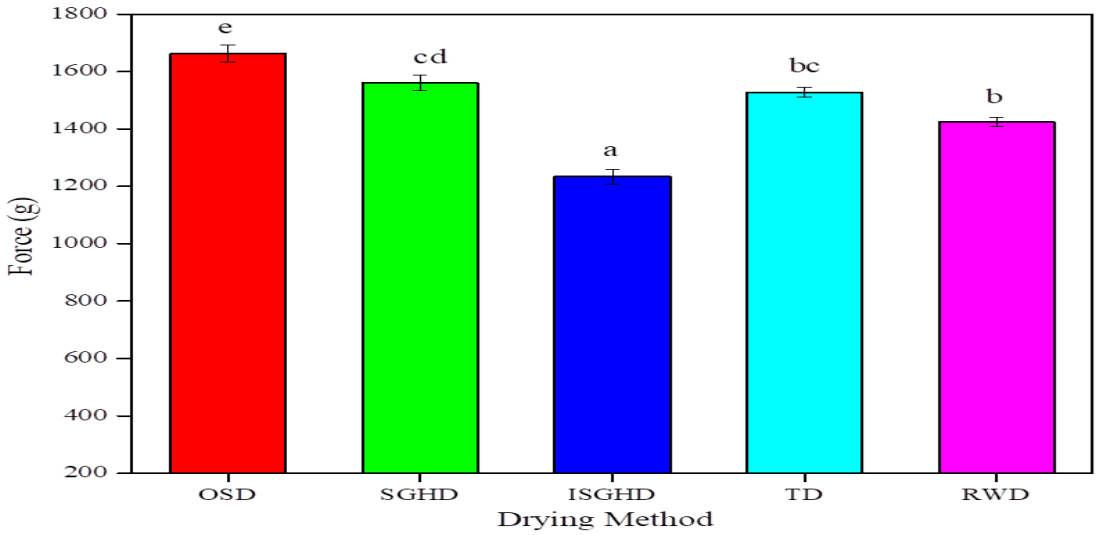

Fig. 4.2.21 Hardness of ginger slices for different drying methods, with different letters (a–e) indicating significant differences ($p < 0.05$)

4.2.8 Essential oil

The extraction of dried ginger essential oil was found to be maximum at 2.1±0.08 % in ISGHD, followed by 1.9±0.18 % in RWD, 1.85±0.14 % in SGHD, 1.8±0.2 % in OSD, and 1.6±0.12 % in TD drying methods.

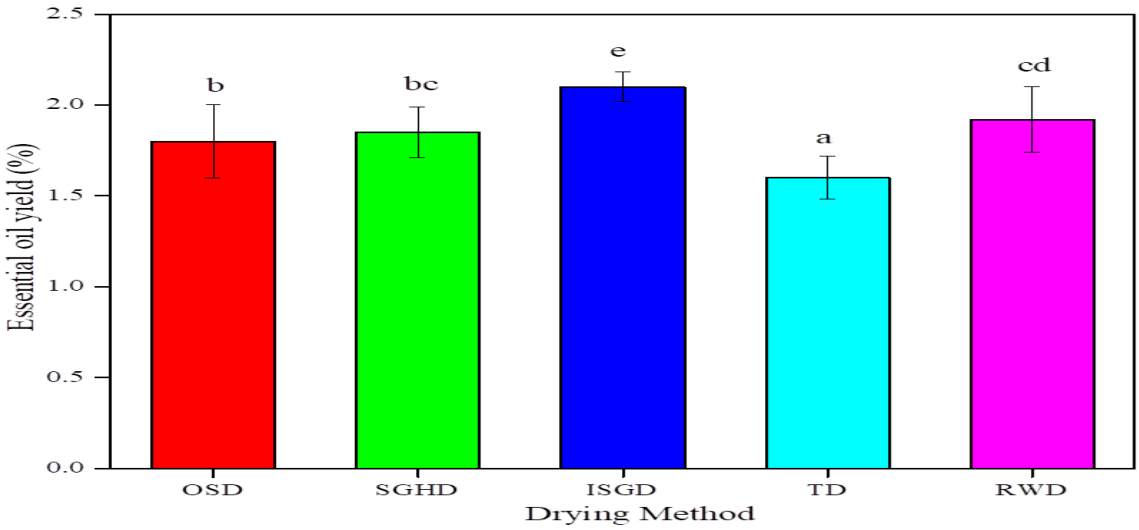

Fig. 4.2.22 Essential oil of ginger slices for different drying methods, with different letters (a–e) indicating significant differences ($p < 0.05$)

The higher efficacy of oil extraction from dried ginger in solar greenhouse drying systems compared to other mechanical drying methods stems from the precise control of temperature within the greenhouse environment, facilitating optimal conditions for oil retention. The gentle moisture removal process in solar greenhouses helps preserve the natural oils present in ginger, ensuring a higher quality of extracted oil, as reported in [86]. Additionally, the reliance on natural sunlight in solar greenhouse drying minimizes the risk of contamination or chemical alteration that may occur with mechanical drying methods utilizing artificial heat sources. (Fig. 4.2.22) shows the essential oil of ginger slices for different drying methods.

4.2.9 Colour properties

In assessing the effectiveness of various drying methods on fresh ginger, including open sun drying (OSD), solar greenhouse drying (SGHD), tray drying (TD), integrated solar greenhouse dryer (ISGHD), refractance window drying (RWD), fresh ginger (FG), distinct colour parameters, such as L*, a*, b*, and ΔE values, were analysed in shown in (Fig.4.2.23).

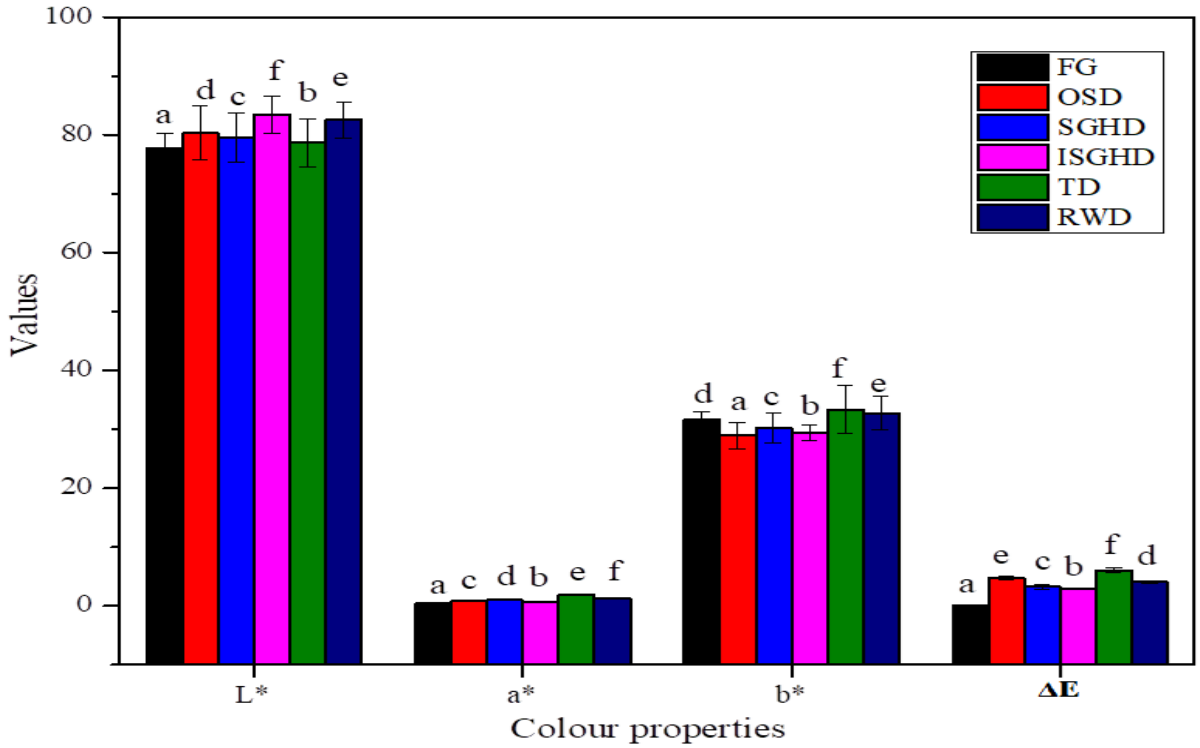

Fig. 4.2.23 Colour properties of ginger slices for different drying methods, with different letters (a–f) indicating significant differences ($p < 0.05$)

OSD demonstrated L* values of 80.33±0.23 and 82.56±3.1. In contrast, SGHD showed values of 79.56±4.10 and 77.71±2.5, respectively, with TD slightly lower at 78.68±4.1 and ISGHD recording the highest at 83.5±3.2. For a* parameter, OSD exhibited 0.80±0.10, SGHD 1.01±0.07, TD 1.94±0.06, and ISGHD 0.62±0.13, while RWD and FG had values of 1.26±0.05 and 0.46±0.08, respectively. Regarding b* values, OSD had 28.90±0.24, SGHD 30.21±2.5, TD 33.37±4.12, ISGHD 29.40±1.25, RWD 32.75±2.8, and FG 31.71±1.3. The overall colour difference (ΔE) was 4.77±0.33 for OSD, 3.24±0.45 for SGHD, 6.02±0.35 for TD, 2.92±0.18 for ISGHD, and 4.02±0.25 for RWD. ISGHD exhibited the minimum ΔE, suggesting reduced browning reactions or inhibition during the drying process, possibly due to controlled drying conditions and reduced oxygen exposure, presenting a similar tendency for ginger compared to other methods, as similar reported for ginger [83,87].

4.2.10 Antioxidant properties

Fig. 4.2.24 shows various parameters of antioxidant properties presented for various drying methods, including open sun drying (OSD), solar greenhouse drying (SGHD), integrated solar greenhouse dryer (ISGHD), refractance window drying (RWD), tray drying (TD), and fresh ginger (FG).

Total phenolics content (mg GAE/g) were as follows: OSD recorded 3.75±0.32, SGHD had 4.1±0.41, ISGHD exhibited 5.42±0.58, RWD showed 5.79±0.30, TD displayed 3.41±0.48, and FG showed 5.9±0.56. Total flavonoids content (mg R/g) were: OSD showed 360.66±8.52, SGHD had 412±10, ISGHD exhibited 430±21.22, RWD recorded 395.62±16.18, TD showed 370±7.2, and FG displayed 388±15. Additionally, DPPH (%) values were: OSD resulted in 72.42±4.5, SGHD had 77±4.8, ISGHD exhibited 83±3.6, RWD showed 80.54±0.81, TD had 73±5.2, and FG displayed 80±4.1. These findings collectively indicate that ISGHD demonstrates exceptionally high values for TPC, TFC, and DPPH, suggesting its efficacy in preserving the antioxidant properties of ginger during the drying process, as showing similar tendency for ginger [58].

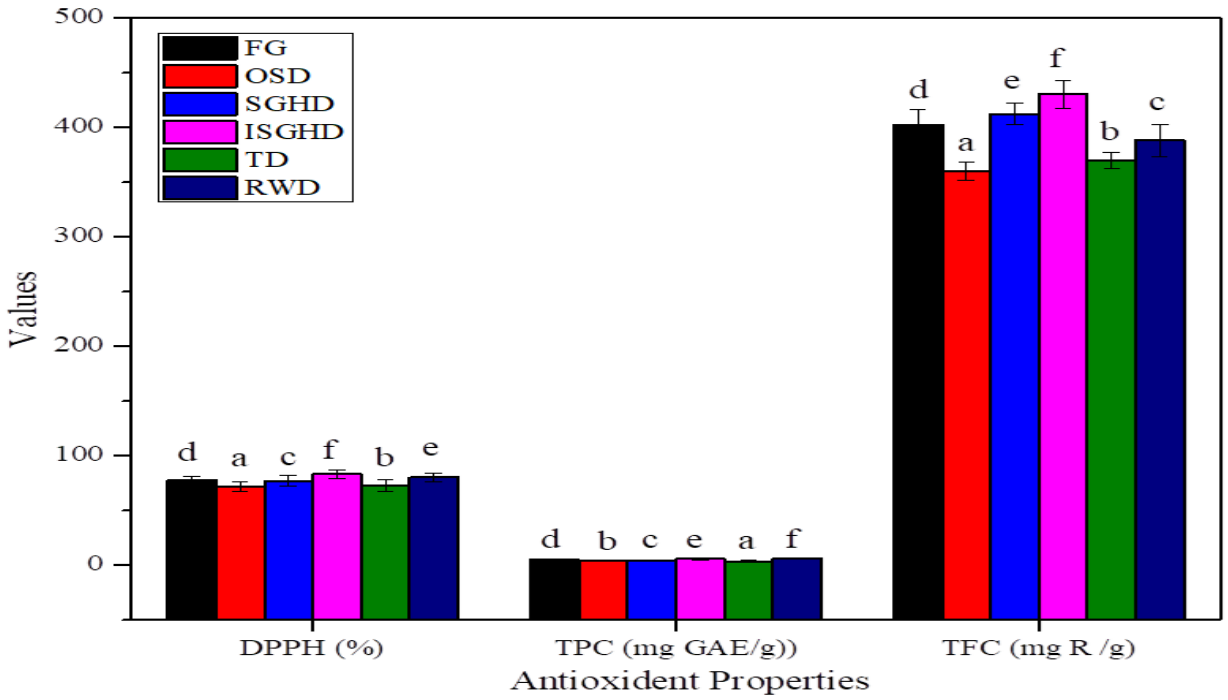

Fig. 4.2.24 Antioxidant properties of ginger powder under different drying methods, with different letters (a–e) indicating significant differences ($p < 0.05$)

4.2.11 X-ray diffraction (XRD)

The XRD analysis distinguished peak angles for different drying methods: integrated solar greenhouse drying (ISGHD), refractance window drying (RWD), and solar greenhouse drying (SGHD) showed peaks at 23.68° 23.65° and 23.60°, indicating significant crystallinity with an amorphous nature, as similar reported in [61,88].

In contrast, TD and OSD had lower angles of 17.57° and 17.57°, respectively. The higher angles in ISGHD and RWD suggest a unique structure likely due to controlled drying conditions, contrasting with the more traditional methods of TD and OSD. The intensity of the peak can reflect the changes in protein structure content. The X-ray diffraction pattern of ginger powder for different drying methods, as shown in Fig. 4.2.25.

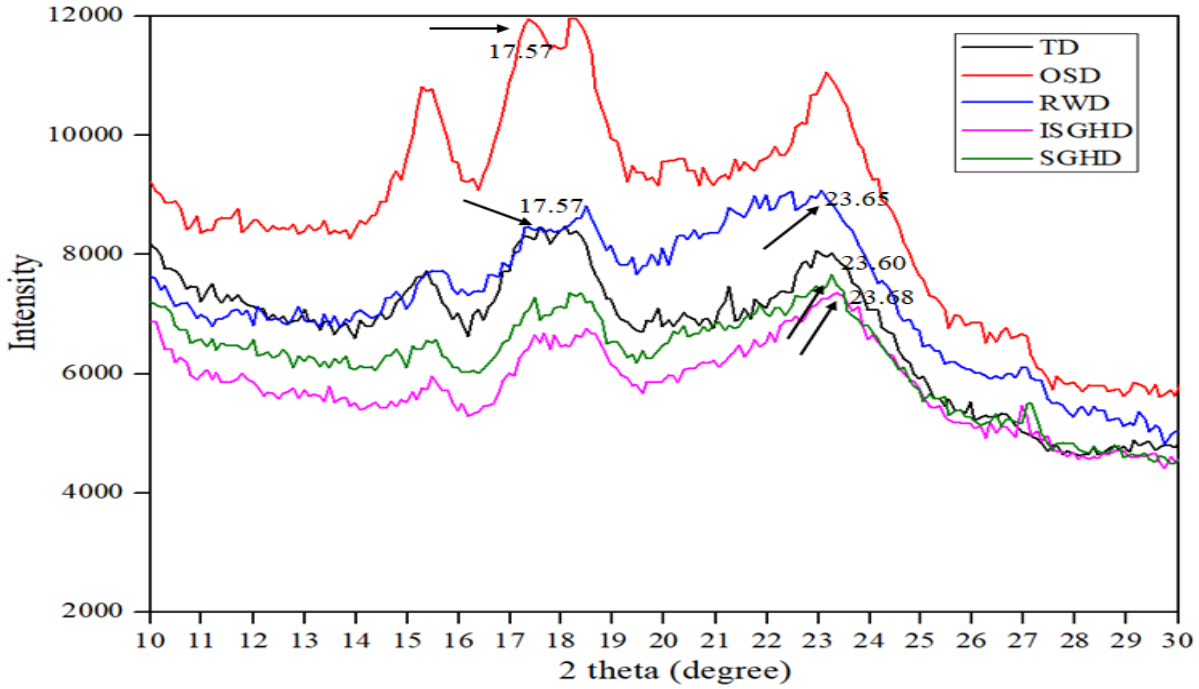

Fig. 4.2.25 X-ray diffraction pattern of ginger powder for different drying methods

4.2.12 Fourier transform infrared (FTIR)

In FTIR, a common feature across various drying methods is the presence of a broader band at the wavelength of 862 cm^{-1}, indicating C-H stretching. Additionally, characteristic bands were identified: 1155 cm^{-1} for C=O and C-O-C stretching, 1516 cm^{-1} for skeleton stretching, and 1639 cm^{-1} for H_2O. These bands offer vital insights into the molecular composition and structural changes occurring during the drying process. The presence of the C-H stretching band at 862 cm^{-1} suggests the involvement of hydrocarbon compounds, likely originating from the agricultural produce being dried. The distinct peaks at specific wavelengths enable researchers to analyze and compare the chemical compositions of various drying methods, aiding in understanding the mechanisms and efficiency of different drying techniques in preserving agricultural products. Fig. 4.2.26 shows the Fourier transform infrared spectra of ginger powder for different drying methods.

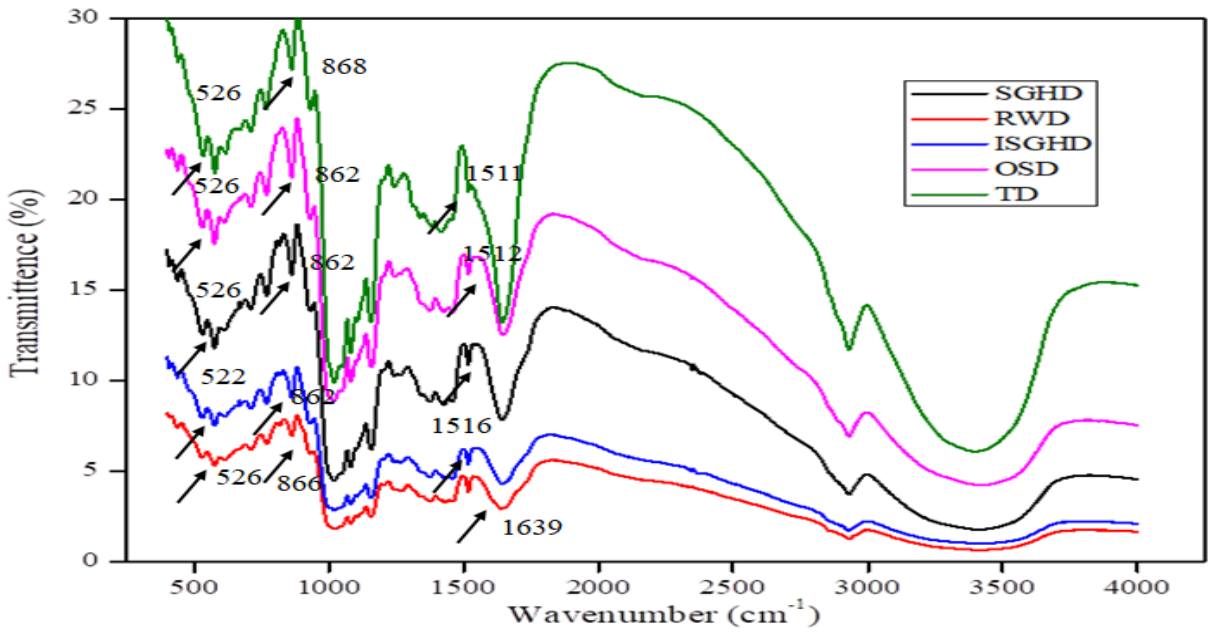

Fig. 4.2.26 Fourier transform infrared spectra of ginger powder for different drying methods

4.2.13 Scanning electron micrograph (SEM)

SEM micrographs of ginger samples dried using different methods, including open sun drying, OSD (Natural convection), solar greenhouse drying, SGHD (Passive mode), integrated solar greenhouse drying, ISGHD (Active mode), refractance window drying (RWD), and tray drying (TD), revealed distinct structural differences. In particular, ginger samples dried by ISGHD and RWD exhibited well-preserved and complete cell structures compared to OSD, SGHD and TD methods. This preservation of cell structure is attributed to the less extreme heating conditions reported during ISGHD and RWD, as similar tendency reported for ginger [83,85,89]. The observed retention of cell structure in ISGHD and RWD ginger samples resulted in the creation of a porous and spongy structure, minimizing structural damage and preventing shrinkage and collapse of cell walls. SEM analysis of ginger for different drying methods, as depicted in Fig. 4.2.27.

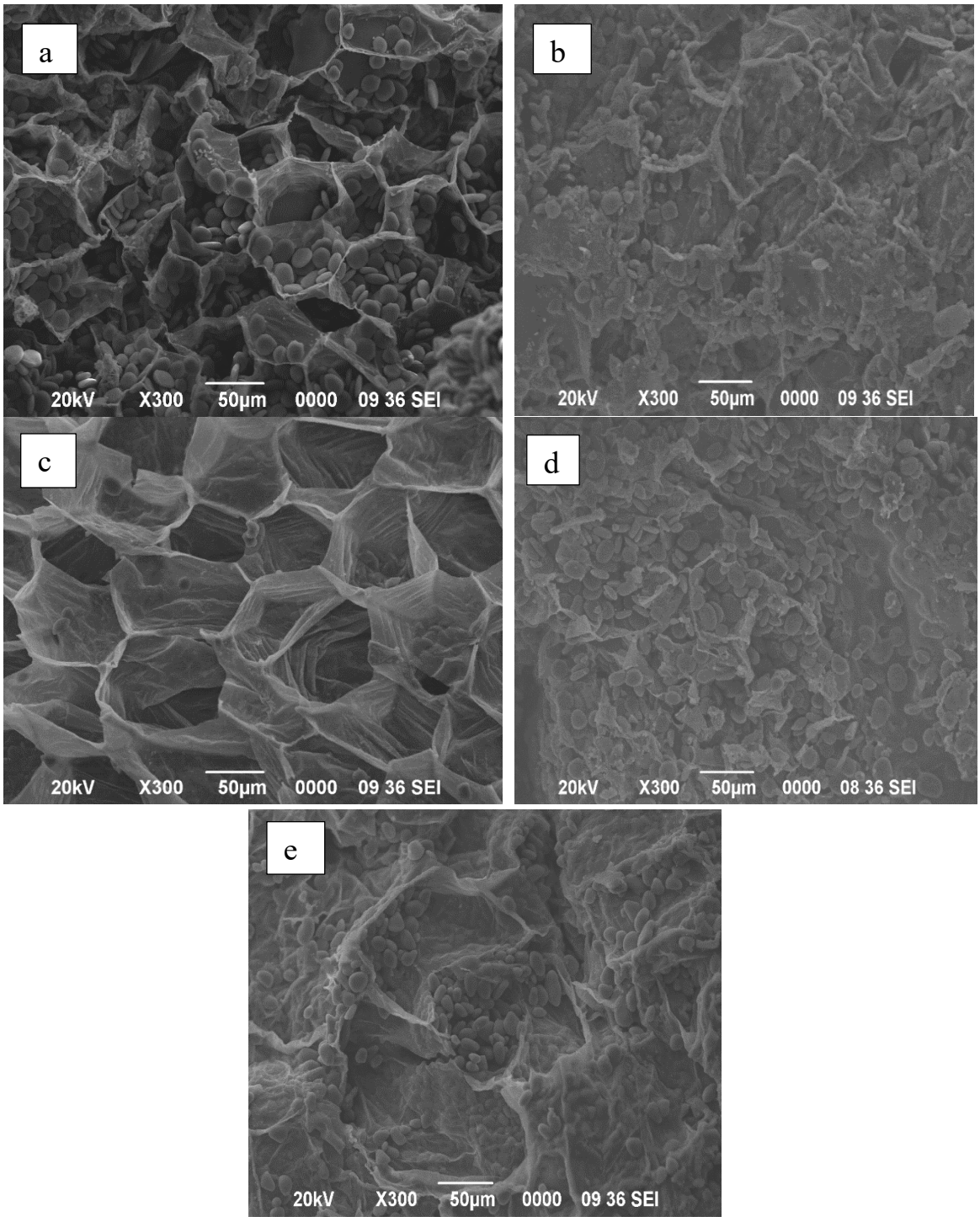

Fig. 4.2.27 Scanning electron micrographs of (a) OSD, (b) SGHD, (c) ISGHD, (d) TD, and (e) RWD

4.3 Thermal performance of solar air heating (corrugated type SAH) and developed ISGHD drying system

4.3.1 Energy rate analysis

4.3.1.1 Solar air heating system (Corrugated type SAH)

Fig. 4.3.1 represents values of energy input (W), energy output (W), and energy loss (W) for corrugated type SAH at various air flow rates.

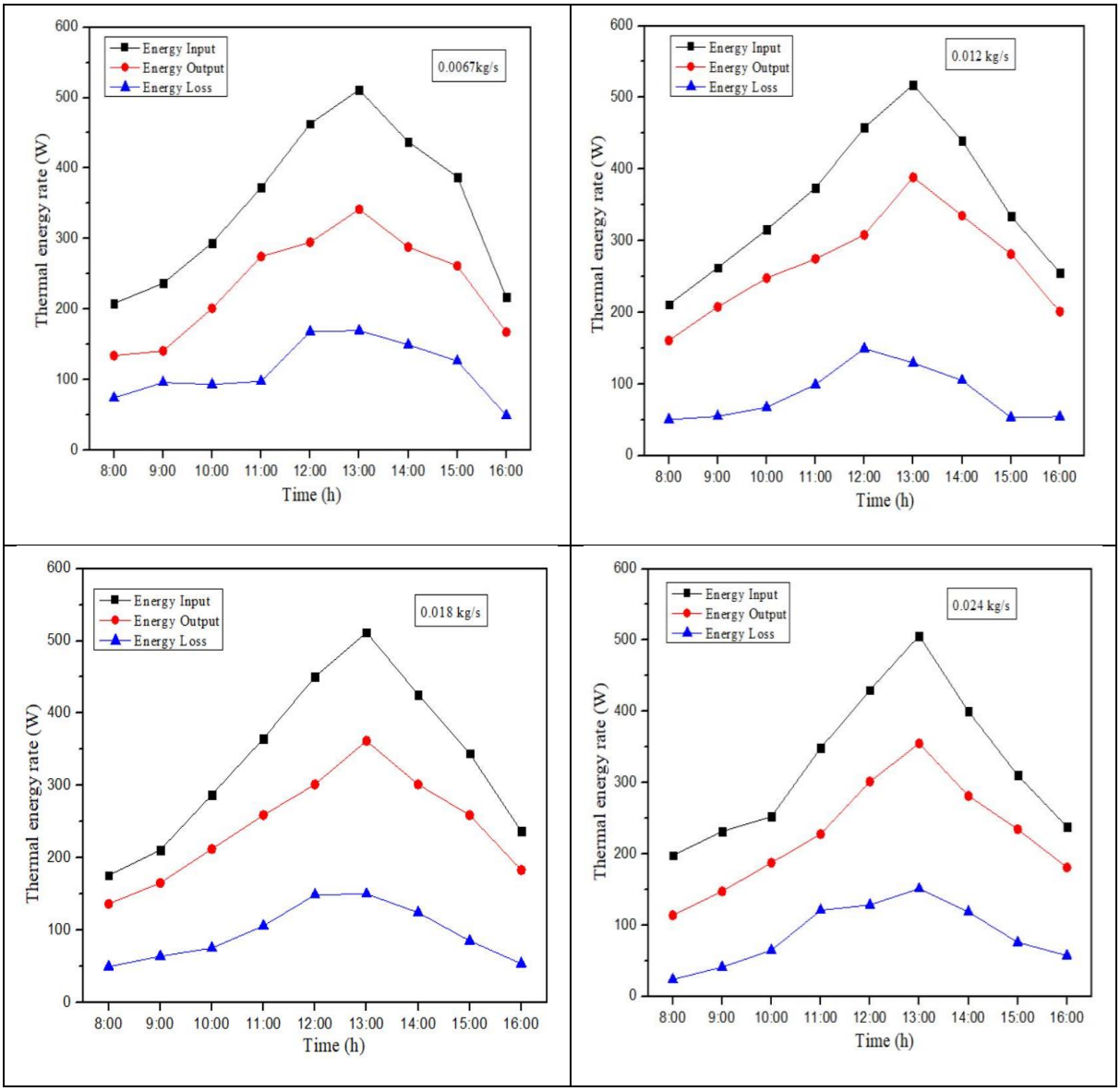

Fig. 4.3. 1 Thermal energy rate of corrugated type SAH at various mass flow rates

For a natural flow rate of 0.0067 kg/s, the energy input varies from 208 to 511 W, with corresponding energy outputs of 134 to 341 W and energy losses of 74 to 169 W. For airflow rate of 0.012 kg/s, the energy input ranges from 211 to 517 W, while the energy output ranges from 160 to 388 W, and the energy loss ranges from 50 to 129 W. Similarly, at MFR of 0.018 kg/s and 0.024 kg/s, the energy input, output, and losses vary within specified ranges. These values provide insights into the performance of the SAH system across various operating conditions. In (**Appendix- A**), given all values of energy analysis for SAH.

The thermal performance of a corrugated type SAH was examined across various flow rates. Results indicated that the highest thermal efficiency, ranging from 38% to 63%, was achieved at a mass flow rate of 0.018 kg/s. Subsequently, efficiencies of 34% to 57%, 36% to 53%, and 33% to 47% were recorded at MFR of 0.012 kg/s, 0.024 kg/s, and 0.0067 kg/s, respectively, as depicted in (Fig. 4.3.2). These results highlight that the SAH system performs best at intermediate flow rates.

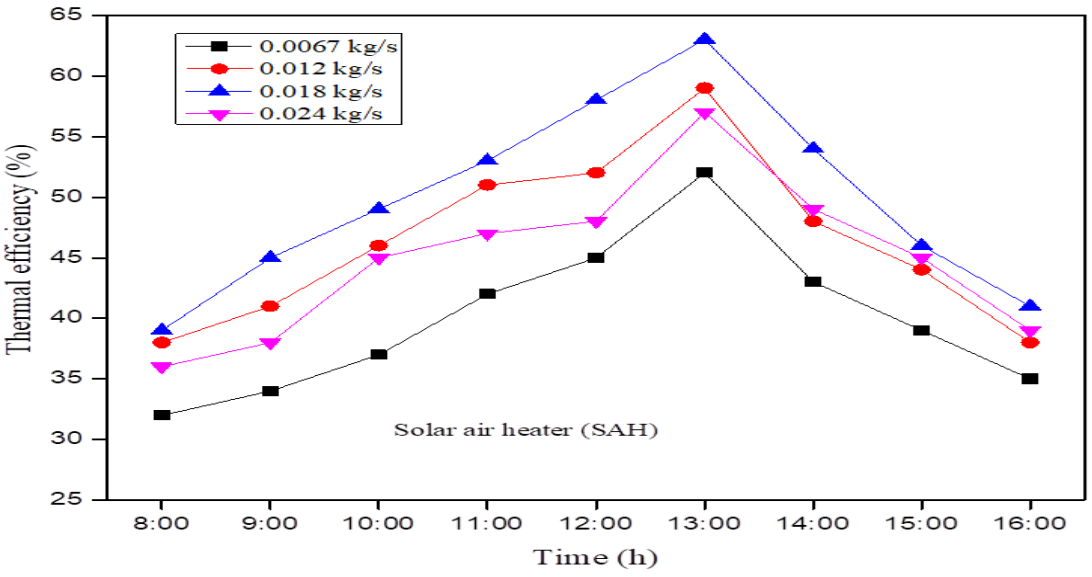

Fig. 4.3.2 Thermal efficiency of corrugated type SAH at various mass flow rates

4.3.1.2 Integrated solar greenhouse drying system (ISGHD)

Fig. 4.3.3 illustrates the values of energy input (W), energy output (W), and energy loss (W) for an integrated solar greenhouse drying system (ISGHD) at various air flow rates. For a natural flow rate of 0.0067 kg/s, the energy input ranges from 198 to 490 W, with corresponding energy outputs

of 140 to 374 W and energy losses of 58 to 116 W. At an airflow rate of 0.012 kg/s, the energy input varies between 195 and 510 W, with energy outputs from 148 to 412 W and energy losses between 47 and 98 W. Similarly, for flow rates of 0.018 kg/s and 0.024 kg/s, the energy input, output, and losses exhibit variability within specified ranges.

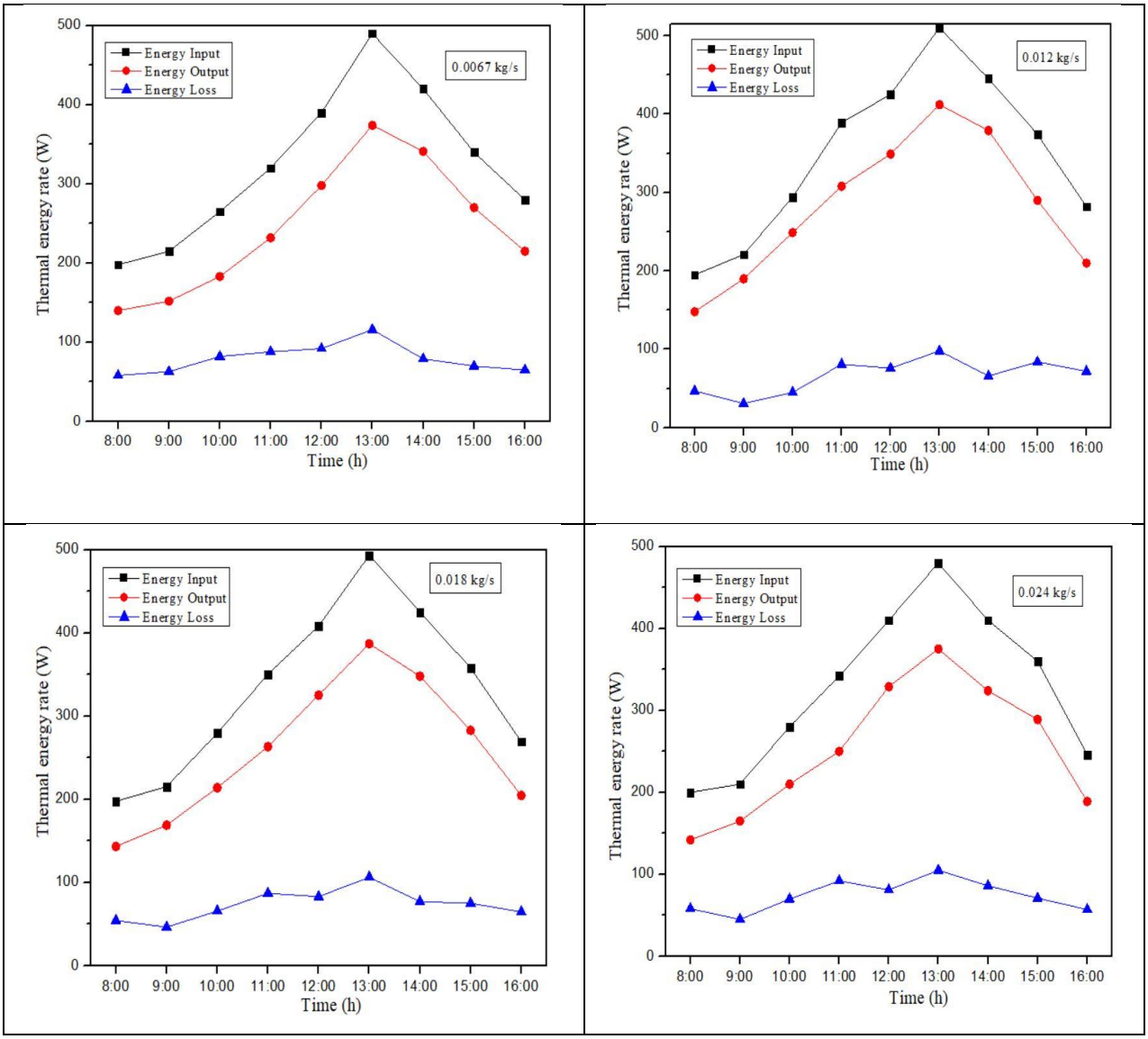

Fig. 4.3.3 Thermal energy rate of ISGHD system at various air flow rates

The thermal performance of the integrated solar greenhouse drying system (ISGHD) at various flow rates was examined. (Fig. 4.3.4) shows that the ISGHD dryer achieved maximum thermal efficiency of 33-45% at 0.018 kg/s, followed by 29-41% at 0.012 kg/s, 27-41% at 0.024 kg/s, and

24-49% at 0.0067 kg/s. These findings highlight the impact of flow rate on the efficiency of the ISGHD system, with optimal performance generally occurring at intermediate flow rates.

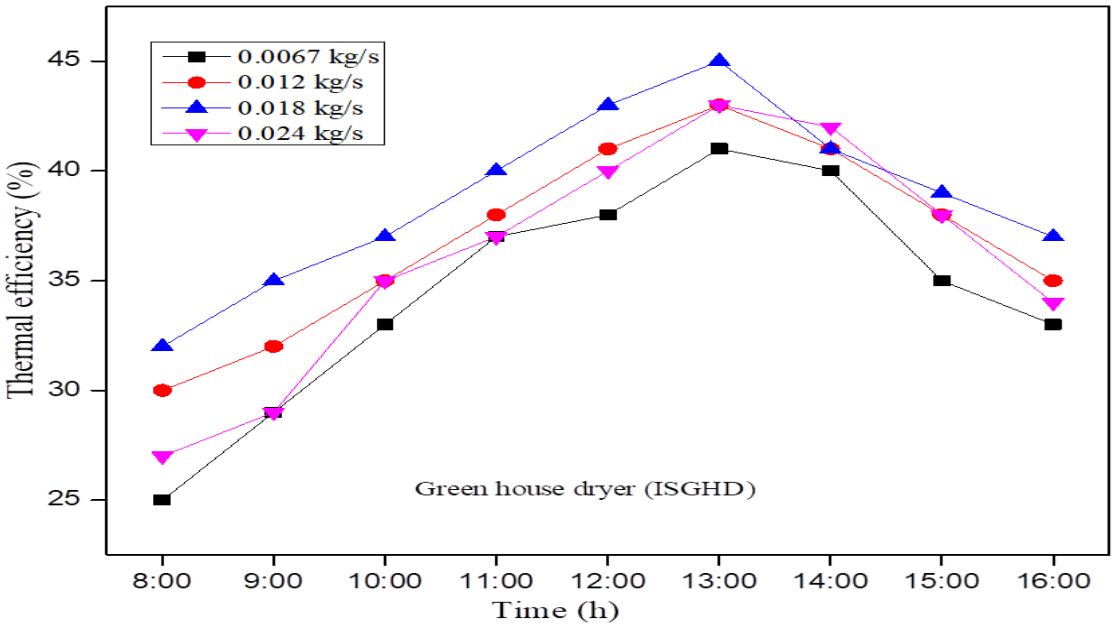

Fig. 4.3.4 Thermal efficiency of ISGHD at various flow rates

4.3.2 Exergy rate analysis

Fig. 4.3.5 displays the values of exergy input (W), exergy output (W), and exergy loss/useful (W) for the integrated solar greenhouse drying system (ISGHD) at various air flow rates. For a natural flow rate of 0.0067 kg/s, the exergy input ranges from 34 to 134 W, with corresponding exergy outputs of 3.0 to 31 W and exergy loss/useful of 32 to 106 W. At MFR of 0.012 kg/s, the exergy input varies between 31 and 144 W, with exergy outputs ranging from 6 to 45 W and exergy loss/useful between 25 and 98 W. Similarly, for MFR of 0.018 kg/s and 0.024 kg/s, the exergy input, output, and losses exhibit variability within the specified ranges. Experimental data shows that the highest exergy destruction occurred at 12:30 p.m. when the sun's light was at its highest. Experimental data shows that the highest exergy destruction occurred at 12:30 p.m. when the sun's light was at its peak, primarily due to increased heat transfer and thermal losses within the system. Additionally, this temperature differential can lead to increased exergy destruction as the system works to maintain temperature equilibrium and manage heat transfer processes.

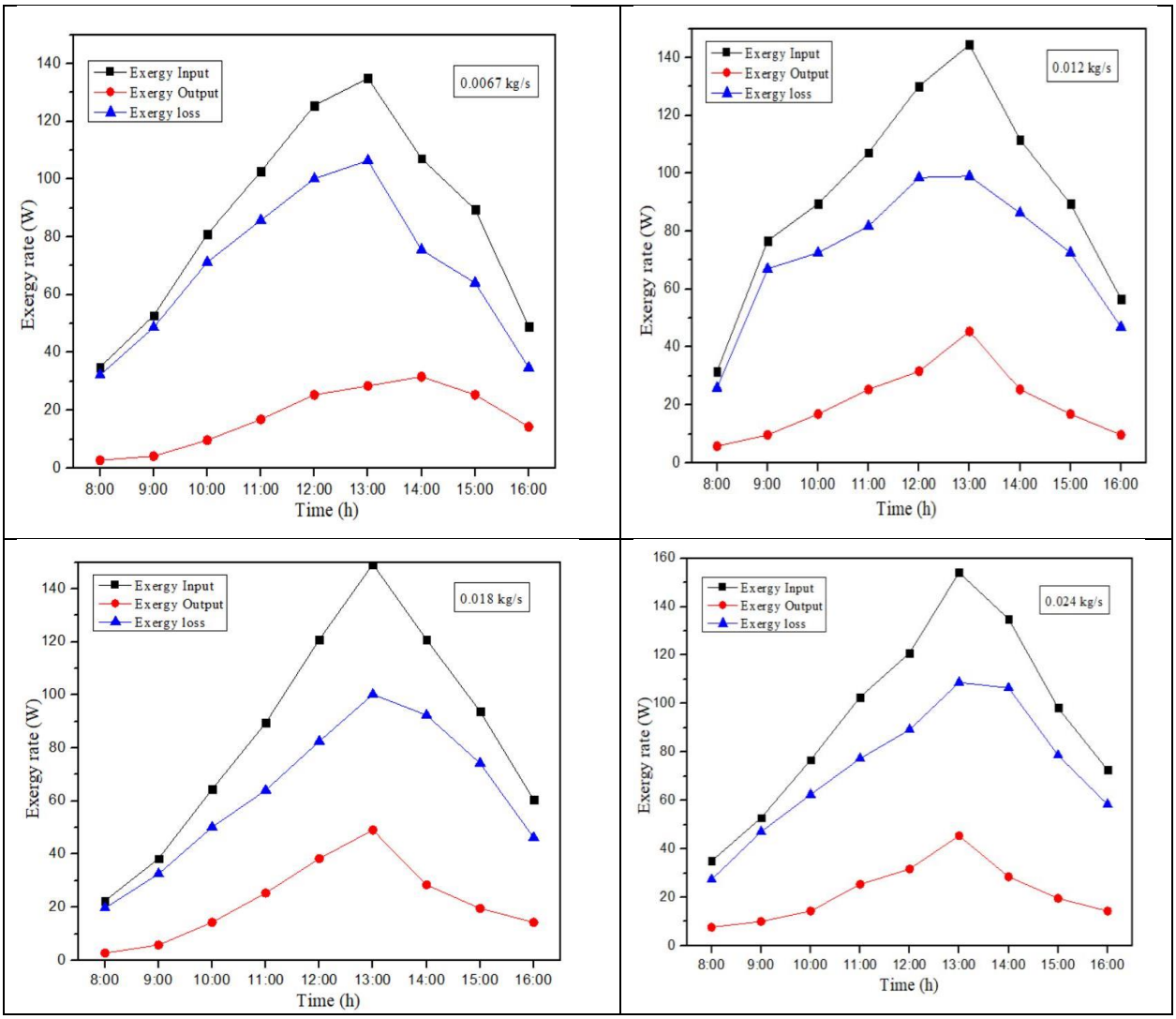

Fig. 4.3.5 Exergy input, exergy output and exergy loss of ISGHD at various flow rates

The variance in exergy efficiency of the ISGHD system is depicted in (Fig. 4.3.6). The highest exergy efficiency of the ISGHD dryer was observed to be 12-33% at MFR of 0.018 kg/s, followed by 13-30% at 0.012 kg/s, 14-28% at 0.024 kg/s, and 8-28% at 0.0067 kg/s. These findings show that ISGHD system exergy efficiency peaks at intermediate flow rates.

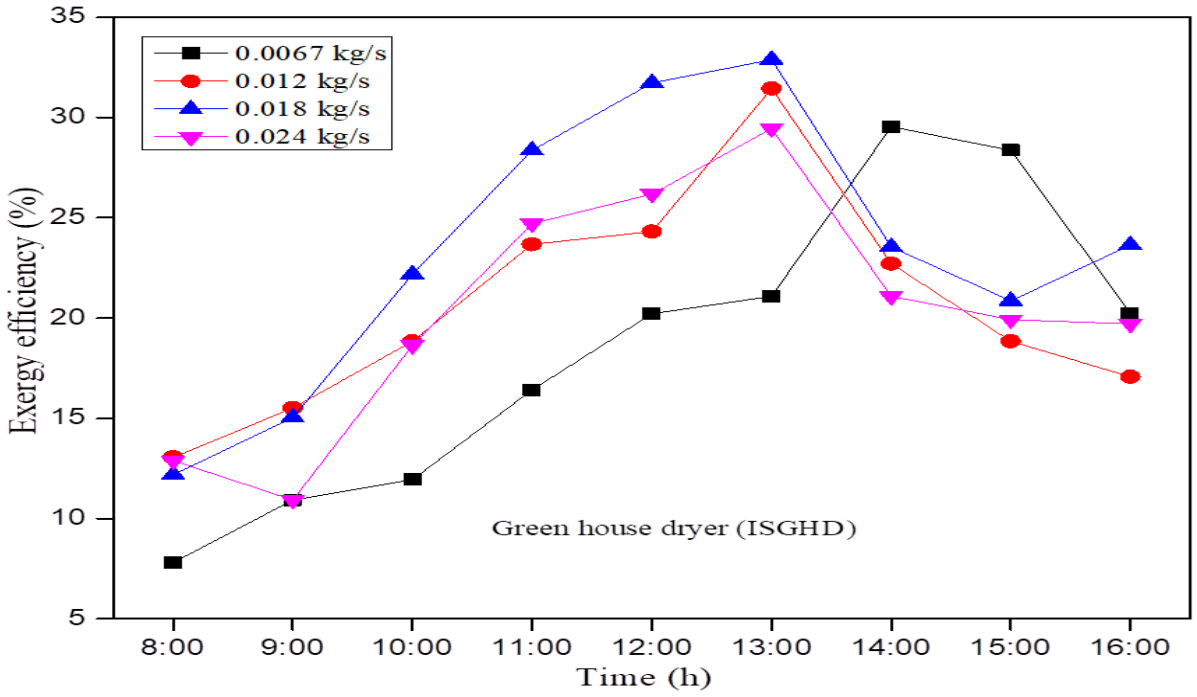

Fig. 4.3.6 Exergy efficiency of ISGHD at various mass flow rates

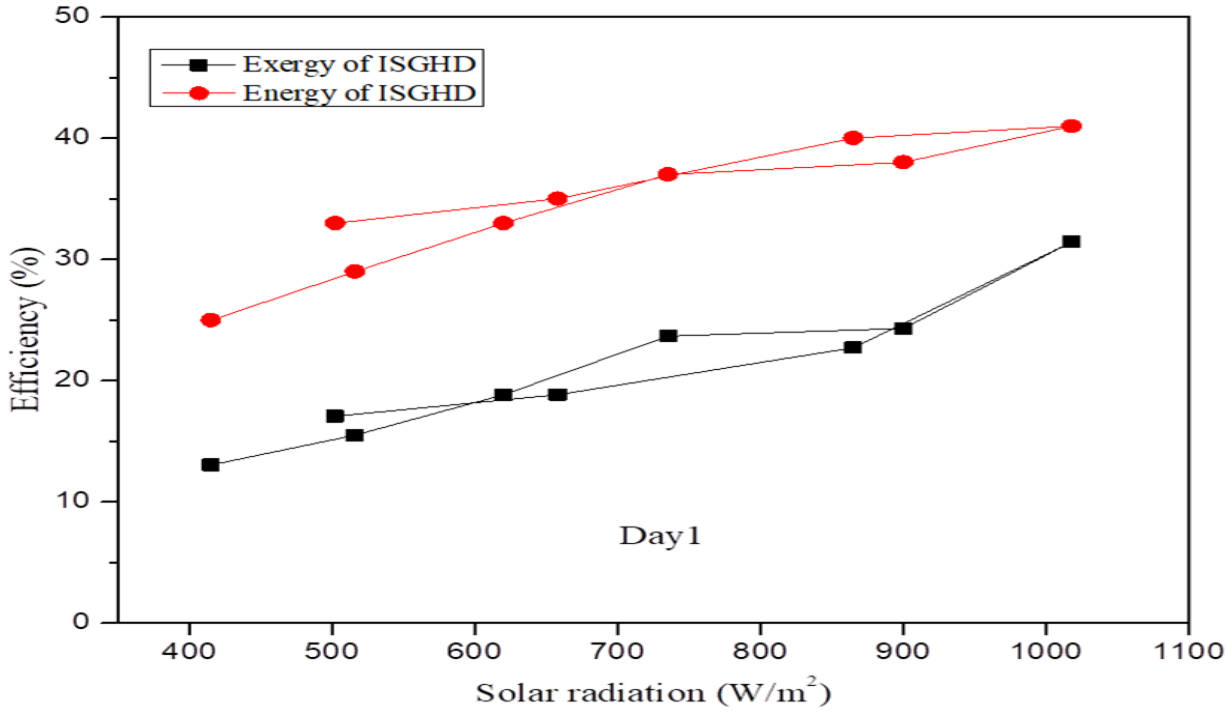

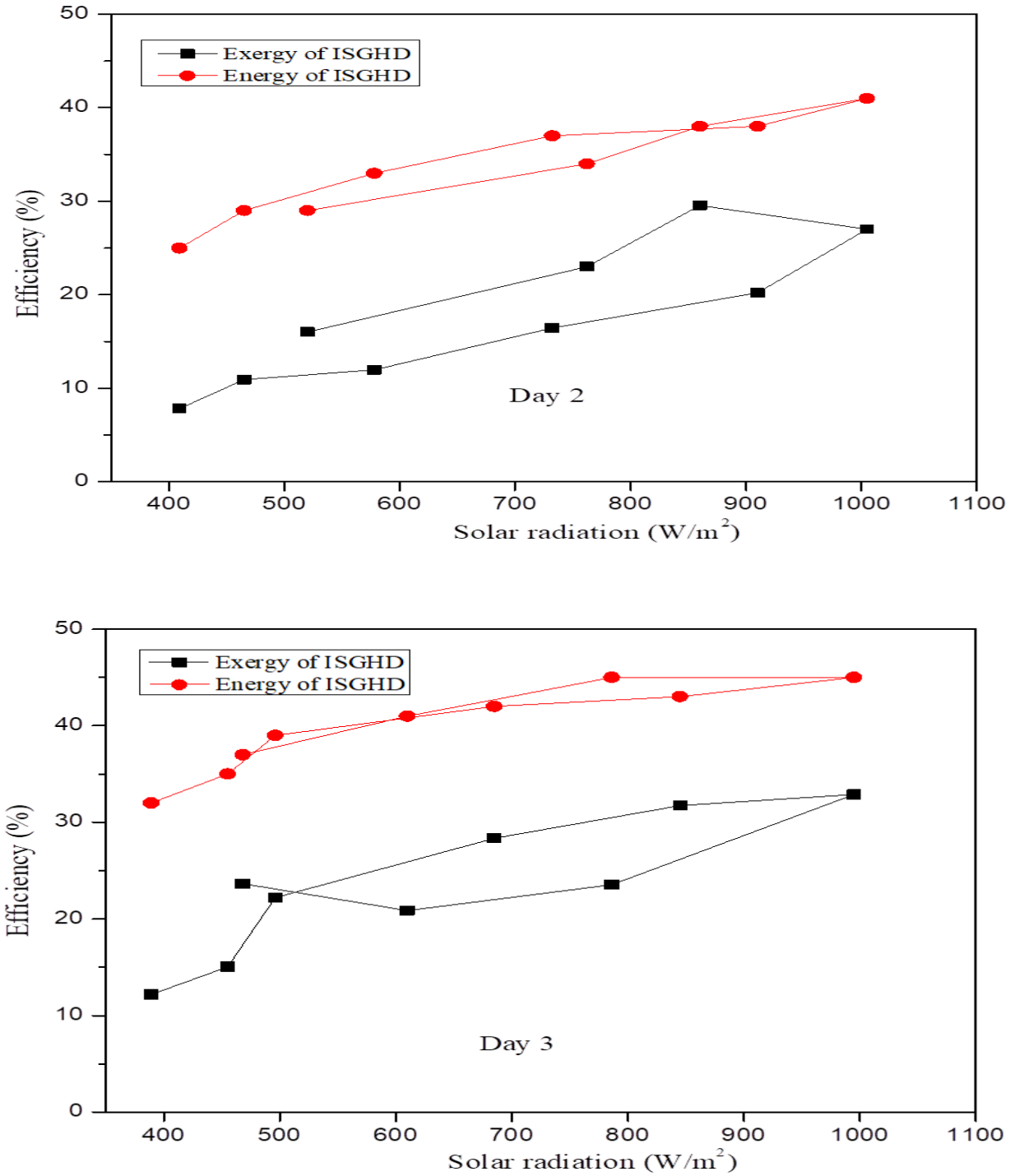

Fig. 4.3.7 Energy and exergy efficiency of ISGHD over three consecutive days with respect to solar radiation

The energy and exergy efficiency of an integrated solar greenhouse drying system (ISGHD) were analyzed over three consecutive days, concerning the solar radiation received each day, as shown

in (Fig. 4.3.7). Maximum energy efficiency ranged from 24% to 45%, while maximum exergy efficiency ranged from 12% to 33%. Table 4.3.1 shows the overall performance of corrugated SAH and developed ISGHD.

Table 4.3.1 Shows the performance of SAH and ISGHD system for ginger drying

Particulars	Values
Weight of ginger sample (kg)	4
Initial moisture content, w.b. (%)	86
Final moisture content, w.b. (%)	10
Drying time of ginger in ISGHD (h)	30
Drying temperature (^{o}C)	55-60
Thermal efficiency of the SAH (%)	38-63
Thermal efficiency of the Overall dryer (ISGHD) (%)	24-45
Specific energy consumption (kWh/kg)	4-6
Exergy inflow of ISGHD (W)	4-19
Exergy outflow of ISGHD (W)	0.5-11.5
Exergy efficiency of ISGHD (%)	12-33

4.3.3 CFD simulation for ginger drying

Studying the drying process of ginger slices in an ISGHD and validating the simulation results with experimental data is crucial for optimizing the process. Simulation helps visualize temperature distribution and airflow, allowing for a better understanding of how these factors affect drying kinetics and slice quality [94].

To begin the simulation process in COMSOL Multiphysics 5.2a, the first step is to import the 3D geometry of the greenhouse dryer model, which has been previously designed in CATIA. Once imported, the next step involves generating a mesh for the computational domain within the COMSOL software. This mesh creation is crucial for accurately representing the geometry and facilitating the numerical calculations required for the simulation, as shown in (Fig. 4.3.8). In the geometry domain also indicated the thermocouple fixed inside the greenhouse domain, as shown in (Fig. 4.3.9).

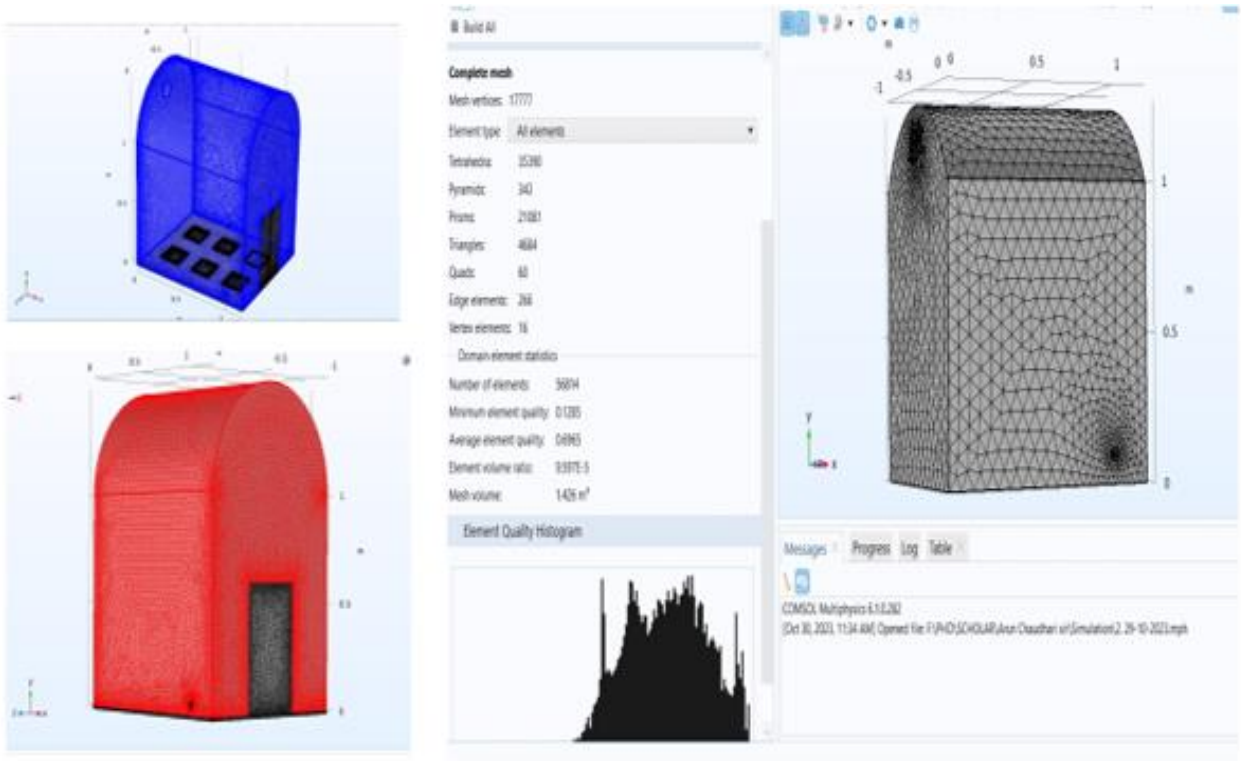

Fig. 4.3.8 Generated mesh for the computational domain for ISGHD

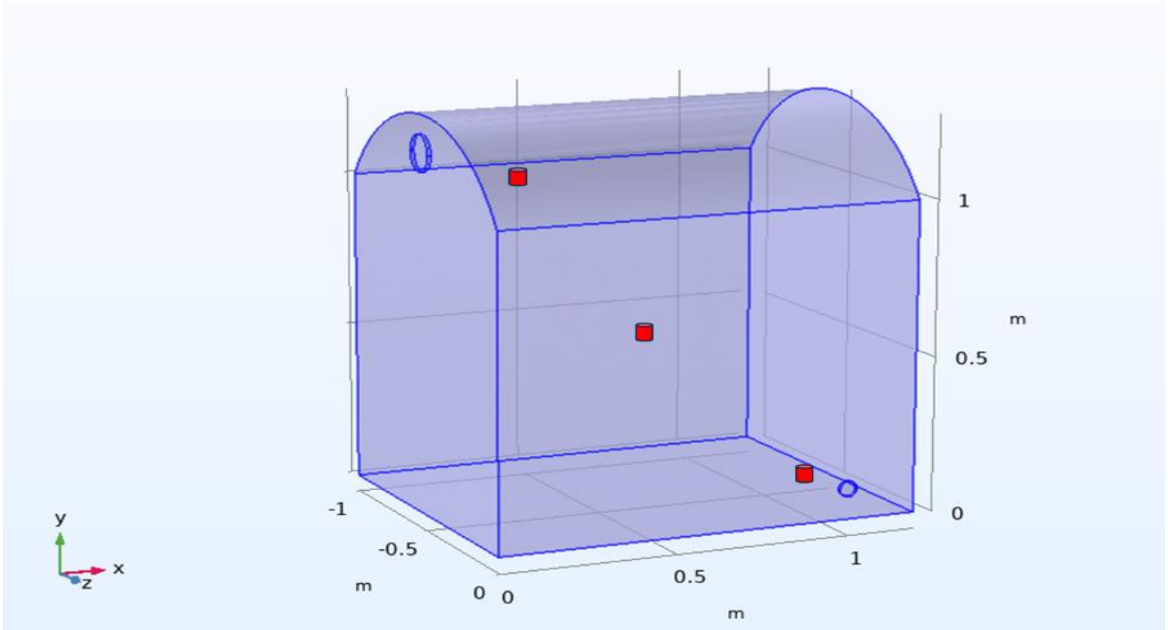

Fig. 4.3. 9 Thermocouple placed inside the drying chamber during the experiment

With the mesh generated, the simulation setup can proceed, focusing on incorporating the k-ε turbulence model. This model is commonly used for simulating turbulent flow in fluid dynamics, providing insights into the complex behaviours of the airflow within the greenhouse dryer. (Fig. 4.3.10) & (Fig. 4.3.11) shows the air turbulence flow inside the drying chamber of ISGHD.

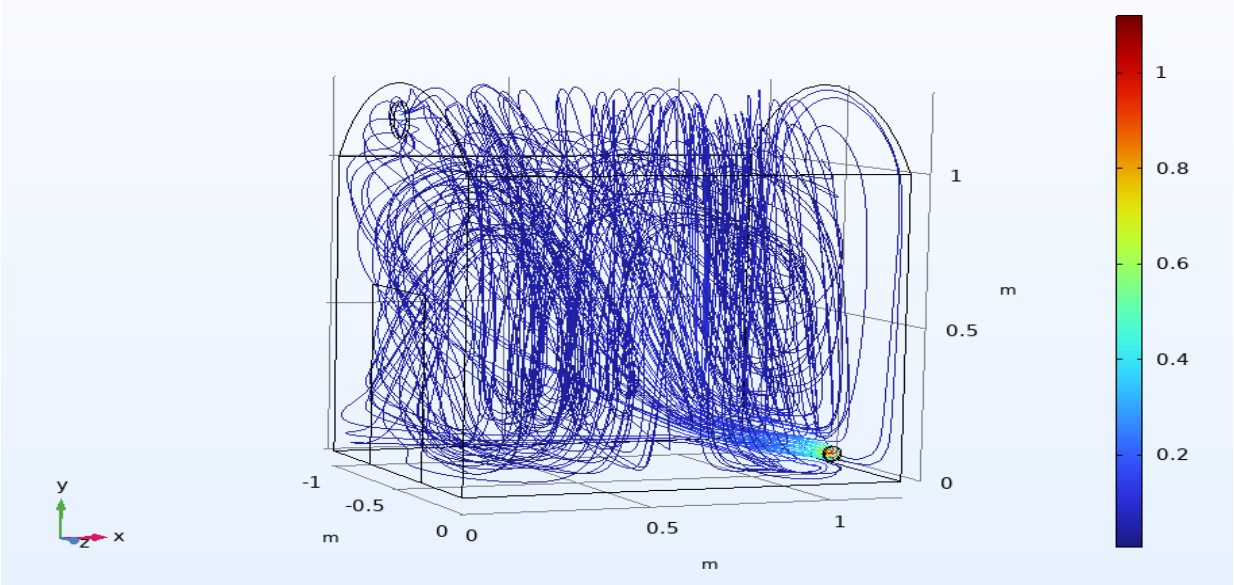

Fig. 4.3.10 Air turbulence flow inside the drying chamber of ISGHD

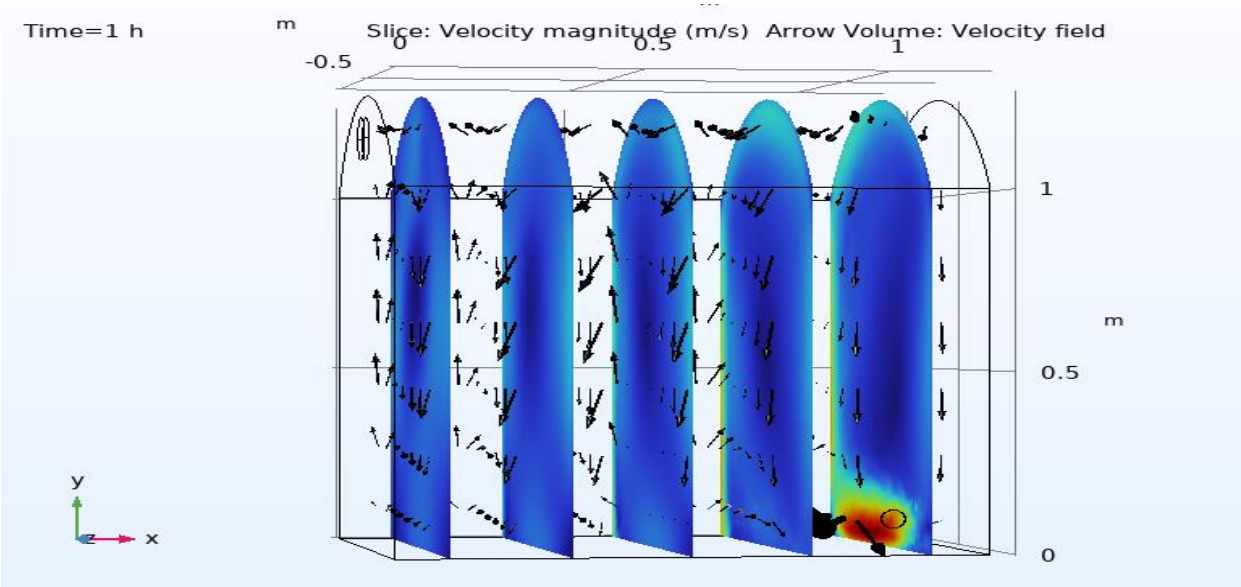

Fig. 4.3.11 Air profiling inside the drying chamber of ISGHD

The temperature distribution over time within the solar greenhouse drying (ISGHD) system has been simulated, considering an airflow rate of 0.018 kg/s within the drying chamber. This computational approach enables the prediction of temperature profiles throughout the drying process. By incorporating the principles of heat transfer and fluid dynamics, the simulation captures the dynamic behaviours of temperature within the dryer structure. The predicted temperature distribution offers valuable insights into the thermal performance of the ISGHD, as shown in (Fig. 4.3.12). The experimental vs simulated temperature of drying chamber of ISGHD graph shown in (Fig. 4.3.13).

<table>
<tr><td> 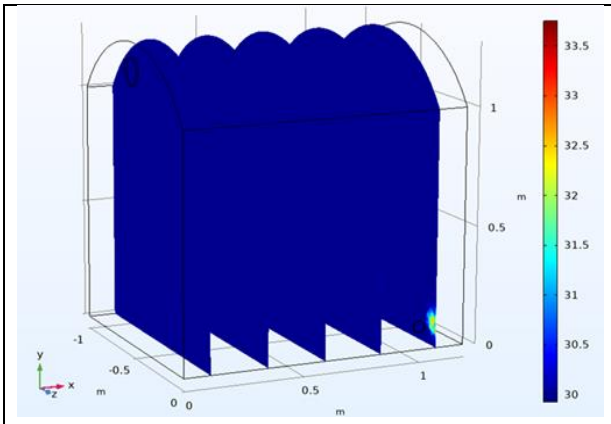
</td><td> 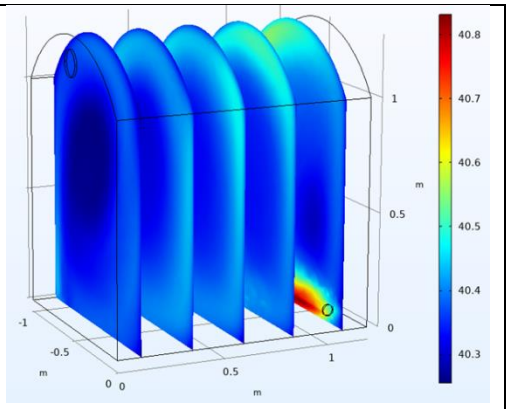
</td></tr>
<tr><td>8:00 a.m.</td><td>9:00 a.m.</td></tr>
<tr><td> 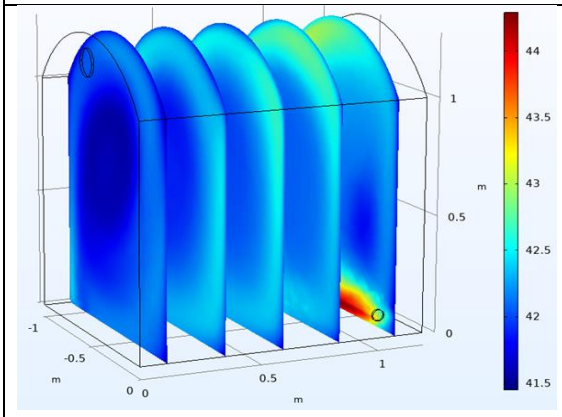
</td><td> 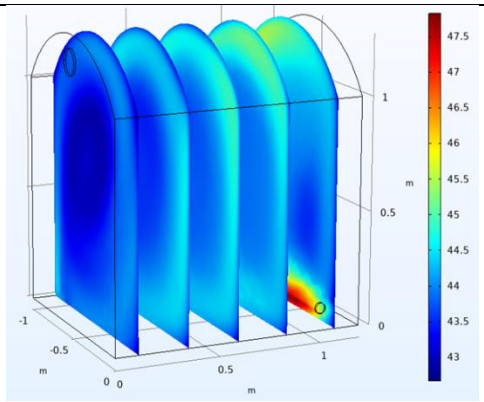
</td></tr>
<tr><td>10:00 a.m.</td><td>11:00 a.m.</td></tr>
</table>

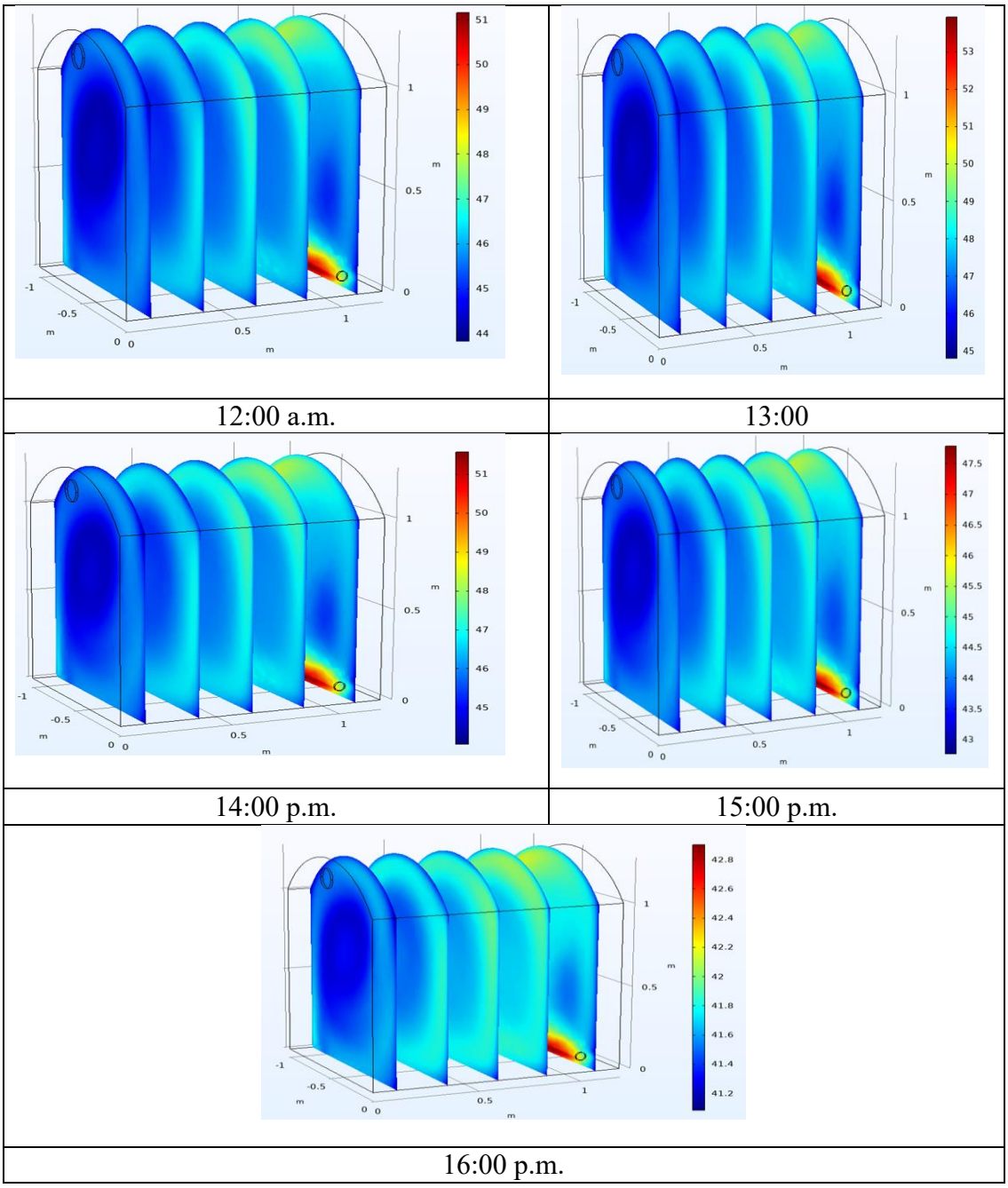

Fig. 4.3.12 Temperature distribution vs time in solar greenhouse dryer at 0.018 kg/s air flow rate

Simulation allows for exploring various scenarios to optimize temperature, airflow rates, and slice thickness for efficiency and quality. Validation through comparison with experimental data enhances confidence in the predictive model. Ultimately, the simulation aims to provide insights into ginger slice drying in an ISGHD system, facilitating better process control and optimization for enhanced efficiency and product quality [100].

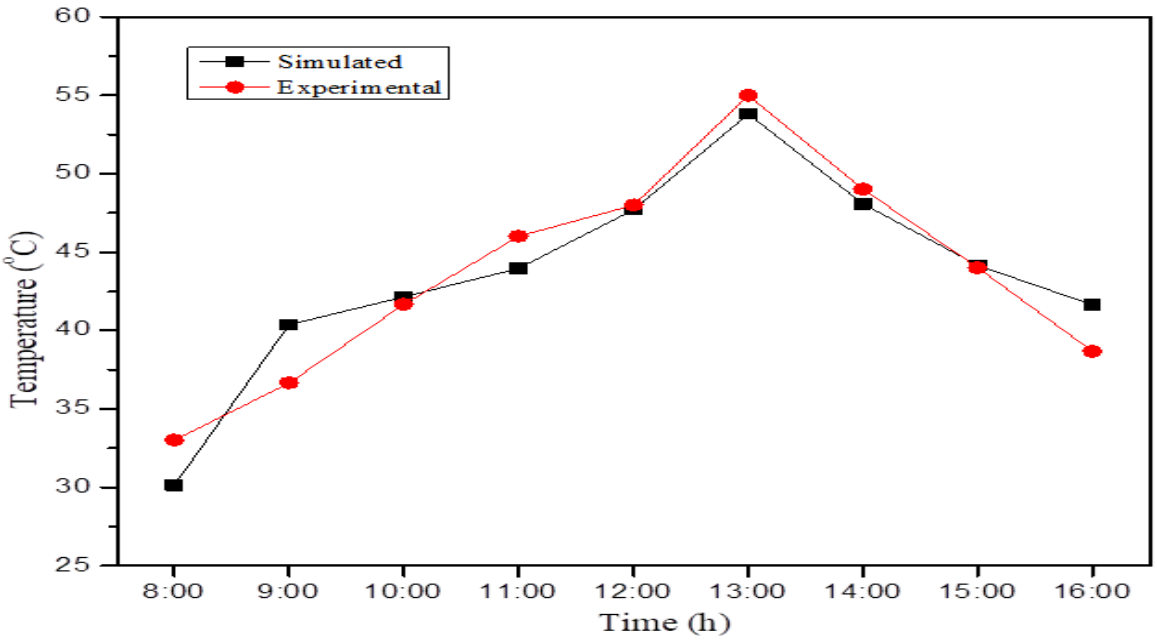

Fig. 4.3.13 Simulated and experimental temperature value inside the drying chamber at 0.018 kg/s air flow rate

4.3.4 Uncertainty analysis

Uncertainty is an examination of the unpredictability and error in finding values. Uncertainty of the instrument calibration calculation using by (Eq. 3.40 – Eq. 3.42). Table 4.3.2 gives the uncertainty parameter during the experiment was observed.

Table 4.3.2 Uncertainty of the parameters during the experiment of ginger drying

Parameters	Uncertainty
Temperature (°C)	±0.328
MFR of air (kg/s)	±0.01
Solar radiation (Wm^{-2})	±2.0
Relative humidity (%)	±1.4
MC (kg water/kg dry matter)	±0.5
Weight loss (g)	±0.01
Energy efficiency of SAH (%)	±3.2
Energy efficiency of ISGHD (%)	±4.1

4.4 Environmental and cost analysis

4.4.1 Environmental

The integrated solar greenhouse drying (ISGHD) system demonstrates a commendable environmental profile, exemplified by its total embodied energy of 1199.442 kWh and an energy payback time (EPBT) of 2.33 years. These figures underscore its efficiency and sustainability, as the energy invested in its production is recuperated in a relatively short timeframe. Furthermore, the dryer's annual CO_2 emissions stand at 470.18 kg, a significant reduction compared to conventional drying methods. This reduction is facilitated by its energy-efficient design and reliance on solar power. Notably, the ISGHD achieves an impressive carbon mitigation rate of 2.042 kg/kWh, resulting in a net carbon mitigation of 1422 kg per year. These translate into tangible environmental benefits, such as reducing the carbon footprint associated with food drying processes. Table 4.4.1 shows the total embodied energy for creation of integrated solar greenhouse dryer (ISGHD). Dryer component embodied energy distribution chart for developed ISGHD is shown in Fig.4.4.1. The calculation of environmental parameter gives in (**Appendix-B**).

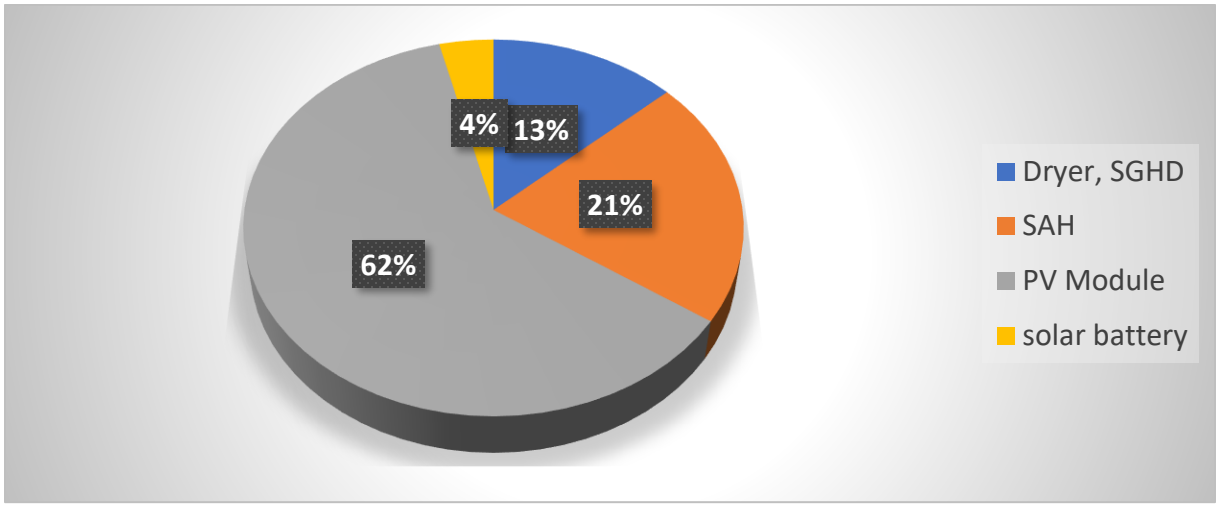

Fig. 4.4.1 Embodied energy percent distribution chart of ISGHD

Additionally, the dryer's energy requirement per day per batch is a modest 0.1024 kWh, contributing to its sustainability credentials. With a total annual consumption of 19.456 kWh, the ISGHD represents a low-impact solution for food preservation, minimizing both energy usage and environmental harm. Moreover, the dryer's carbon credits, totalling 5332 INR, provide an

economic incentive for its adoption, further incentivizing sustainable practices. In summary, the ISGHD emerges as an environmentally sound and economically viable solution, offering a pathway towards greener and more efficient food drying technologies. (Table 4.4.2) gives a detailed view on carbon dioxide emission, mitigation, and carbon credits.

Table 4.4.1 Embodied energy under integrated solar greenhouse drying (ISGHD)

S. No	Material	Weight (kg)	Embodied energy coefficient (kWh/kg)	Total (kWh)
1	Dryer			
	UV stabilized polyethylene	2.0	19.25	38.5
	Black polyethylene sheet	0.25	19.44	4.88
	Bamboo pillar	5.0	20.6	103
	Steel tray	0.75	9.67	7.25
	Mild steel binding wire	0.10	9.23	0.923
	DC fan	0.25	19.44	4.86
2	Solar air heater			
	Glass cover	1.0	7.28	7.28
	Corrugated GI sheet	1.5	9.636	14.44
	Cast iron	20	6.99	139.8
	Glass wool	1.0	4.044	4.044
	Paraffin wax	5.0	9.1	45.5
	PVC pipe	1.5	19.39	29.085
	DC exhaust fan	0.12	19.44	2.33
	Paint	0.5	25.11	12.55
3.	PV module	-		739
4	Solar battery	-		46
		Total		1199.442

Table 4.4.2 Carbon dioxide emission, mitigation, and carbon credits

S. No	Parameters	Amount
1	Embodied energy (kWh)	1199.442
2	Energy payback time (year)	2.33
3	CO_2 emission per year (kg)	470.18
4	CO_2 Mitigation per Year (kg/kWh)	2.042
5	CO_2 mitigation lifetime (kg)	2449
6	Net carbon mitigation (kg)	1422
7	Carbon credits earned (INR)	5,332

4.4.2 Economic analysis

The developed integrated solar greenhouse drying (ISGHD) system not only demonstrates impressive environmental benefits but also proves to be economically advantageous. For the creation of ISGHD many items are required, as given detailed with cost in Table 4.4.3.

Table 4.4.3 Cost analysis for the developed ISGHD

S. No	Items	Description	Unit cost (INR)	Total Cost (INR)
1	UV stabilized Polyethylene	2.0	400	800
2	Black polyethylene sheet	0.10	20	20
3	Bamboo pillar	5.0 no.	50	250
4	Steel tray	4.0 no.	40	160
5	GI Binding Wire	100g	20	20
6	DC fan	1.0 no.	250	250
7	Glass cover	1.0 no.	100	100
8	Corrugated GI sheet	0.5 kg	200	200
9	Cast iron	20 kg	50	1000
10	Glass wool	100g	10	10
11	Paraffin wax	5.0 kg	100	500
12	PVC pipe	2.0 no.	50	100
13	DC Exhaust fan	1.0	275	275
14	Paint	0.5 kg	100	50
15	PV Module	1.0	1500	1500
16	Solar battery	1.0	100	1000
		Total		6235

In (Appendix-B) given detailed for economic analysis with calculation. With an annual energy cost of 116.736 INR and a specific cost of drying per kg at 29.184 INR, the dryer offers efficient operation at a reasonable expense. Additionally, the annual capital cost of the dryer amounts to 6733 INR, with a salvage value (S_v) of 3358 INR, indicating a manageable initial investment as shown detailed in Table 4.4.4. Furthermore, considering the annual cost of dryer operation, which includes depreciation and salvage value, totaling 3575 INR, the ISGHD proves to be financially sustainable over time.

Table 4.4.4 Economic evaluations of the developed ISGHD

S. No	Parameter	Value
1	Dryer capacity (kg)	4
2	The energy requirement of (kWh) SGHD/day/ batch	0.1024
3	Energy Requirement per kg (kWh)	0.0256
4	Total Annual Consumption (kWh)	19.456
5	Annual Energy Cost (INR)	116.736
6	Specific cost of drying per kg (INR)	29.184
7	Capital Cost of the dryer (INR)	6733
8	Salvage value (INR)	3358
9	Duration of life of dryer (year)	10
10	Rate of interest per year	6%

4.5 Summary of chapter IV

Intensity of solar radiation, air velocity, ambient temperature and relative humidity, which vary according to location are crucial parameters for the development of solar air heating and the integrated solar greenhouse drying (ISGHD) systems. Subsequently, these ambient parameters significantly affect the progression of drying of crops and produces in the ISGHD. Season specific variation of these parameters in the experiment site were air temperatures ranged from 19-33°C with 55-92% humidity in summer (March to June), whereas corresponding values in winter (October to February), were 15-27°C with 38-72% relative humidity.

The development of a (i) corrugated SAH with PCM and (ii) ISGHD system, with heated air produced by the developed SAH with PCM and circulated by a PV module operated air circulation system is discussed in this chapter. PCM is utilized as LHS system within the SAH to maintain the

drying air temperature during the off-sunshine hours for minimum 3 - 4 hours. Black-painted rocks and sand were used to serve as a sensible heat storage system (SHS) integrated within the drying chamber, which effectively increased the chamber temperature by 2-3 °C. Both LHS within SAH and SHS within the drying chamber function as TES, helped to significantly enhance the efficiency of the dryer and accelerate the drying rate.

When the outlet temperature of the SAH and ISGHD system is checked under no-load conditions, the outlet temperature varied with mass flow rate of air, with the maximum temperature being observed between 12:00 to 1:00 p.m. Optimal temperature conditions were observed at MFR of 0.018 kg/s, indicating a superior efficiency and reduced drying time.

It was observed that as the chamber temperature increases, relative humidity (RH) decreases following the psychrometric behaviour of moist air. Lower RH levels signify improved drying efficiency and reduced drying time, underscoring the significance of controlling airflow rates for enhanced drying performance in the ISGHD system.

The ISGHD was used to dry fresh ginger with 84% moisture to a safe moisture level of 10%. Drying characteristics such as the variation of MC, MR, and DR for ginger slices with thicknesses of 3.0, 5.0, and 7.0 mm slices were measured experimentally. The same behaviour was studied using various other drying methods such as OSD, SGHD, ISGHD, TD, and RWD, as well.

For the 3.0 mm slices, the drying times are 54 h, 50 h, 29 h, 17 h, and 15 h in OSD, SGHD, ISGHD, TD, and RWD, respectively. For 5.0 mm slices, the drying times are 59 h, 57 h, 31 h, 20 h, and 18 h in OSD, SGHD, ISGHD, TD, and RWD, respectively. For 7.0 mm slices, the drying times are 77 h, 54 h, 32 h, 22 h, and 19 h in OSD, SGHD, ISGHD, TD, and RWD, respectively.

DR increases as drying air temperature increases and decreases as the drying time of ginger increases. An efficient ISGHD which yields a relatively higher drying air temperature than a SGHD, leads to a faster and shorter drying. Moisture diffusivity (D_{eff}) is a crucial drying parameter, which is higher in ISGHD drying methods.

Ten drying models were used to investigate the drying kinetics for ginger slices, with the Page model showing a strong fit, followed by the logarithmic model and the Newton model. The Page model (R^2=0.99998 and χ^2=0.00016) exhibited a strong fit, trailed by the logarithmic model (R^2=0.99987 and χ^2=0.00032) and Newton model (R^2=0.99447and χ^2=0.00046), were able to

predict the ideal drying behaviour of ginger in the ISGHD drying system. These models effectively represent the drying process and have the potential for practical application in optimizing drying operations.

ANN was utilized to simulate the kinetics of ginger drying. The developed ANN structure had five neurons in the input layer and three neurons in the output layer, with a 5-10-3 architecture chosen for the study of ginger drying.

Higher DPPH, TFC, and TPC values in ginger after drying indicate a more substantial antioxidant potential, which is found under ISGHD. In ISGHD, the rehydration ratio was maximized, shrinkage ratio minimized, essential oil yield optimized, and hardness minimized, indicating its superior performance. In FTIR, the wavelength 862 cm^{-1} showed a C-H stretching broader band that is common in drying methods. In XRD analysis, a high peak at a 2θ value of around 23° signifies the amorphous nature with significant crystallinity of ISGHD and RWD drying method. Additionally, the SEM images of ISGHD samples showed a clear and well-retained fibrous structure.

The thermal performance of both the corrugated type SAH with PCM and the ISGHD system were evaluated at different flow rates of air. The corrugated SAH showed peak efficiency (38%-63%) at 0.018 kg/s flow rate, while the ISGHD system achieved the highest efficiency (24%-45%) at the same flow rate, with an optimal performance at intermediate rates.

The exergy analysis of the ISGHD system showed peak efficiency (12%-33%) at a flow rate of 0.018 kg/s, with highest exergy destruction observed at 12:00-1:00 p.m. during the peak sunlight.

Using the CFD software, the air flow and air temperature profiles were modelled and validated for these parameters within the drying chamber for the drying process of ginger slices in the ISGHD system. There were reasonable agreement of the measured temperature and CFD estimated temperature, which validated the predicted drying time for ginger slices within the ISGHD.

Following the evaluation of the performance of the dryer, environmental and cost analyses of the developed ISGHD system were conducted. The ISGHD system demonstrates a commendable environmental profile, exemplified by its total embodied energy of 1199.442 kWh and an energy payback time (EPBT) of 2.33 years. It represents a low-impact solution for food preservation, minimizing both energy usage and environmental harm.

The annual capital cost of the dryer amounts to 6733 INR, with a salvage value (S_v) of 3358 INR, indicating a manageable initial investment. The ISGHD system proves to be financially sustainable over time.

In conclusion, the ISGHD stands out as a sustainable solution offering both environmental and economic advantages, for its use by rural farmers.